

國立交通大學

光電工程學系碩士班

碩士論文

藉由最佳化 LED 排列方式增進
背光源 LED 波長使用範圍之模型



Optimization of LED Arrangement for
Extending LED Binning Range in Backlight System

研究生：周秉彥

指導教授：黃乙白 副教授

中華民國 一百零一 年 七 月

藉由最佳化 LED 排列方式增進背光源 LED
波長使用範圍之模型

**Optimization of LED Arrangement for
Extending LED Binning Range in Backlight System**

研究生：周秉彥

Student : Ping-Yen Chou

指導教授：黃乙白

Advisor : Dr. Yi-Pai Huang



A Thesis

Submitted to Institute of Electro-Optical Engineering
College of Electrical and Computer Engineering
National Chiao Tung University
in Partial Fulfillment of the Requirements
for the Degree of Master
in

Electro-Optical Engineering

July 2012

Hsinchu, Taiwan, Republic of China

中華民國 一 百 零 一 年 七 月

藉由最佳化 LED 排列方式 增進背光源 LED 波長使用範圍之模型

碩士研究生：周秉彥 指導教授：黃乙白 副教授

國立交通大學 光電工程學系碩士班

摘要

薄型化液晶電視(Slim format LCD-TV)逐漸成為顯示器市場趨勢，此外，因為發光二極體(LED)具有高能量萃取效率、較長使用壽命、不需使用含汞元素和符合綠色能源需求，LED 被視為是下一代背光源的主流。基於製程上的因素影響，整面晶元(wafer)做出來的所有 LED，各項品質和參數會有些許不同，可以根據光波長、光強度和操作電壓來分類，然而，LED 在背光源的使用上，波長的挑選是非常苛刻的，導致目前面臨 LED 無法有效利用、背光源成本無法降低的問題。

本篇論文提出一套分析背光源光學特性系統，來使 LED 能被運用的更有效率。這套系統的操作原理，首先，需要量測單一光源的光線擴散軌跡(Light spread function)與頻譜(spectrum)資訊，再藉由計算光輝度分布、頻譜線性疊加與色彩座標轉換的模擬程序，來獲得整面背光源色彩均勻性及色偏量的結果。此系統的準確度，已經由比對模擬結果與實際成品來獲得驗證，在展示品中，使用了外層螢光發光技術(Remote phosphor technology)，此結構具備厚度薄、壽命長和光源種類可用範圍廣的優點。藉此分析背光源光學特性系統，可輕易獲得不同條件下的背光色偏量，再加以設計可達降低生產成本與光源有效利用的目的。

Optimization of LED Arrangement for Extending LED Binning Range in Backlight System

Master Student: Ping-Yen Chou Advisors: Dr. Yi-Pai Huang

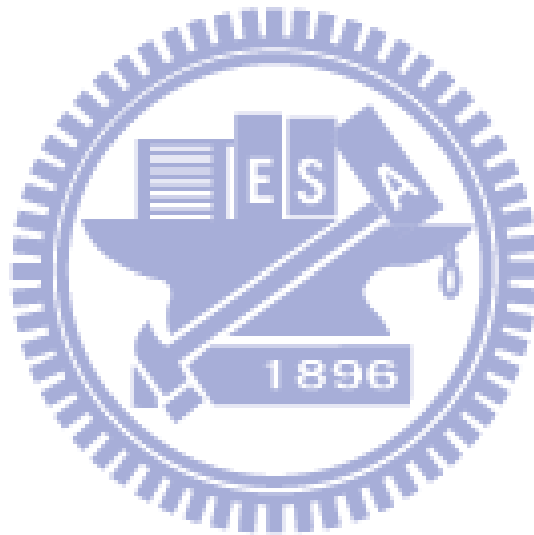
**Institute of Electro-Optical Engineering
National Chiao Tung University**

Abstract

Slim-format LCD-TV had been a trend for the current display market. Moreover, light-emitting diode (LED) is expected to become the backlight source of next generation, because of enhanced energy efficiency, a larger lifetime, the omission of mercury, and compliance with demand for green technologies. Since the manufacturing effect, LEDs are classified to different bin types by wavelength, brightness and voltage. However, the wavelength requirement of LED is very strict in backlight system. Therefore, LED cannot be used effectively in backlight systems, which still have high costs, currently.

In this thesis, an analysis method was developed to calculate the optical properties of direct-emitting backlight systems, which expands the usage of bins. The method based on computing the radiance distribution from the measured light spreading function and spectrum of LED. The calculation procedure includes linear spectral superposition and color difference evaluation. The accuracy of this method was verified by a real backlight module, which introduced the remote phosphor backlight system.

This structure could have more benefits than the traditional one, including thinner thickness, longer life time, and wider LED bins. The conditions of acceptable color deviation values could be simply obtained, and the different binned LEDs could be efficiently used to reduce cost and achieve the wider binned-LEDs application purpose.



誌謝

首先要感謝的是謝漢萍老師與黃乙白老師，在我碩班過程中予我的指導與訓練，包括研究的邏輯思考與組織報告的能力，以及提供良好的研究環境與資源，讓我順利完成論文，獲益良多。

也感謝口試委員們在百忙之中蒞臨，並且不吝嗇地提出寶貴的建議，補足我思考上遺漏的地方。感謝洪健翔學長在研究上細心的指導與協助，在無數次的討論過程中給予我許多實用的意見。在專案合作方面，感謝日本 Sony 公司伊藤博士的協力與幫忙。

實驗室的生活多采多姿，留下許多難忘的回憶。感謝方正學長、國振學長、育誠學長、致維學長、志宏學長、台翔學長、韻竹學姐、柏全學長、奕智學長及精益學長的照顧，還有相同研究領域的姚順以及智清的切磋。一群同甘共苦的同學們，上翰、柏皓、哲軒、博凱、博鈞、綺文、書怡、岡儒以及白諭一起學習與成長的過程，更是我珍貴的回憶。有博元、又儀等其他學長姐和學弟妹們在課業與生活上的陪伴，研究上的辛苦與煩悶隨著歡笑聲而煙消雲散。另外，也感謝實驗室的助理們，為我們學生處理許多重要的事情。

謝謝交大桌球隊的鄭鯤茂領隊、溫景財教練、游鳳芸教練和隊友們，交大光電的同學、學長姐和學弟妹們，系桌的隊友們，因為有你們，豐富了我的生活。

最後感謝家人的支持與鼓勵，讓我無後顧之憂地完成學業。在此致上我最誠摯的感謝。

Table of Contents

摘要.....	i
Abstract.....	ii
誌謝.....	iv
Table of Contents	v
Figure Captions.....	vii
List of Tables	xi
Chapter 1.....	1
1.1 Liquid crystal displays (LCDs)	1
1.2 Direct-emitting backlight systems.....	3
1.3 Remote phosphor technology.....	5
1.4 Motivation and objective	7
1.5 Organization of this thesis.....	9
Chapter 2.....	10
2.1 Geometrical optics in illumination system.....	10
2.1.1 Law of refraction (Snell's law).....	11
2.1.2 Law of reflection.....	12
2.1.3 Fresnel's equations.....	12
2.2 Radiometry	14
2.3 Photometry	16
2.4 Colorimetry	19
2.4.1 CIE 1931 XYZ color space	19
2.4.2 CIE 1976 LUV color space	22
2.5 Summary	24
Chapter 3.....	25
3.1 LSF approximation method.....	25

3.1.1 Light spread function (LSF)	26
3.1.2 Binning factors and spectrums	28
3.1.3 Gaussian binning distribution	32
3.1.4 Convolution	34
3.1.5 Comparing results	34
3.2 Summary	35
Chapter 4	36
4.1 Accuracy of LSF approximation method	36
4.1.1 Correctness of LSF superposition method	37
4.1.2 Tolerance of self-fabricated module	39
4.1.3 Affected color composition range of LED	40
4.1.4 Built-in tolerance from bin width	40
4.1.5 Boundary effect by light reflection	42
4.1.6 Total difference between calculation and experiment	44
4.2 Summary	45
Chapter 5	46
5.1 Random arrangement	46
5.1.1 Results of LEDs random arrangement:	48
5.1.2 Discussion:	55
5.2 Optimized arrangement	56
5.3 Method for reducing gap	60
5.4 Summary	63
Chapter 6	65
6.1 Conclusions	65
6.2 Future works	67
References	68
Publication List	72

Figure Captions

Fig. 1-1 Schematic configuration of a liquid crystal display.	2
Fig. 1-2 Schematic configuration of the conventional backlight systems.	3
Fig. 1-3 Schematic configuration of the conventional direct-emitting backlight systems.	4
Fig. 1-4 Scheme configurations of light emitting diodes.	6
Fig. 1-5 Schematic configuration of (a) conventional direct-emitting backlight and (b) direct-emitting backlight with remote phosphor technology.	7
Fig. 1-6 Usable range of LED binning map for application in direct-emitting backlight.	8
Fig. 2-1 Reflection and Refraction on a boundary surface.....	11
Fig. 2-2 Defining geometry of radiometric quantities.....	15
Fig. 2-3 Scotopic and Photopic spectral sensitivities.....	17
Fig. 2-4 1988 CIE Photopic Luminous Efficiency Function.....	18
Fig. 2-5 Color matching functions $\bar{x}(\lambda)$, $\bar{y}(\lambda)$, and $\bar{z}(\lambda)$ in the CIE XYZ color system.	20
Fig. 2-6 xy chromaticity diagram of CIE XYZ color system.....	21
Fig. 2-7 $u'v'$ chromaticity diagram of the CIELUV color system.	23

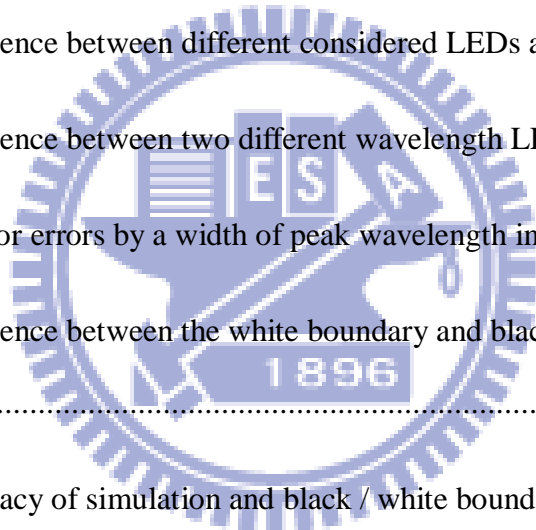
Fig. 3-1 Calculation model flowchart of backlight chromaticity.	26
Fig. 3-2 Measurement setup of light spread function.....	27
Fig. 3-3 Light spread function of single LED illumination with phosphor.	28
Fig. 3-4 CCD camera (ProMetric 1603F-1).....	28
Fig. 3-5 Spectral measurement of binned LED with phosphor film.	29
Fig. 3-6 Different composed blue and yellow light in different locations.....	30
Fig. 3-7 Spectrometer (Topcon SR-UL1R).....	30
Fig. 3-8 Spectrums of blue LED with remote phosphor in different locations.....	31
Fig. 3-9 Spectrums of various binned-LEDs with remote phosphor.....	32
Fig. 3-10 Phosphor emission and excitation data.....	32
Fig. 3-11 Gaussian function with the waist (a) $\sigma=2$; (b) $\sigma=4$, and the ordinals of each bin.	33
Fig. 4-1 Structures of simulated remote phosphor direct-emitting backlight model. ...	37
Fig. 4-2 Ten inch direct-emitting prototype of (a) blue LEDs; and (b) phosphor sheet and optical films with LED illuminating.	37
Fig. 4-3 Spectrums measurement setup with turning on (a) 3×3 LEDs; and (b) 5×5 LEDs.	38
Fig. 4-4 Simulated spectrums superposition compared with measurement data.	38
Fig. 4-5 Measurement deviation by small tilt angle between panel normal and detector.	39

Fig. 4-6 Peak wavelengths of LEDs in the same bin to test the built-in errors.	41
Fig. 4-7 Prototype with white boundary.	43
Fig. 4-8 Prototypes (a) without boundary; and (b) with black boundary.	43
Fig. 4-9 Total differences between simulation and measurement in LUV color space.	44
Fig. 4-10 Effected LEDs light by multi-reflection between reflector and diffuser plate.	45
Fig. 5-1 Amount binned- LEDs of selecting LEDs exactly number method.....	47
Fig. 5-2 Amount binned- LEDs of picking up LEDs randomly method.....	47
Fig. 5-3 Color deviation with $\sigma_1=1$ in selecting LEDs exactly method.....	49
Fig. 5-4 Color deviation with $\sigma_1=2$ in selecting LEDs exactly method.....	49
Fig. 5-5 Color deviation with $\sigma_1=3$ in selecting LEDs exactly method.....	50
Fig. 5-6 Color deviation with $\sigma_1=4$ in selecting LEDs exactly method.....	50
Fig. 5-7 Color deviation with $\sigma_1=1$ in picking up LEDs randomly method.	51
Fig. 5-8 Color deviation with $\sigma_1=2$ in picking up LEDs randomly method.	51
Fig. 5-9 Color deviation with $\sigma_1=3$ in picking up LEDs randomly method.	52
Fig. 5-10 Color deviation with $\sigma_1=4$ in picking up LEDs randomly method.	52
Fig. 5-11 Color deviation with $\sigma_1=1$ in the worst case.	53
Fig. 5-12 Color deviation with $\sigma_1=2$ in the worst case.	53

Fig. 5-13 Color deviation with $\sigma_1=3$ in the worst case.	54
Fig. 5-14 Color deviation with $\sigma_1=4$ in the worst case.	54
Fig. 5-15 Flowchart of the optimized arrangement method.	56
Fig. 5-16 Optimized arrangement of each bin in basic unit array.	57
Fig. 5-17 Arrangement of whole panel with considering boundary effects.....	58
Fig. 5-18 Optical films and illuminating prototype of optimized LEDs arrangement.	59
Fig. 5-19 Enhanced color uniformity of optimized arrangement than random arrangement with fixing (a) total wavelength range; (b) color deviation.	59
Fig. 5-20 Simulated structures with (a) gap=30mm; and (b) gap=10mm.	60
Fig. 5-21 Detected area of analyzed structure in Photometry.....	61
Fig. 5-22 Emitting light shapes of (a) normal LEDs (module gap=30mm); and (b) calculated LEDs (module gap=10mm).	62
Fig. 5-23 Emitting light shape of real LEDs in the commercial when gap=30mm.	62
Fig. 5-24 Emitting light shape of real LED in the commercial when gap=10mm.....	62
Fig. 5-25 Simulated illuminances in software with 30mm and 10mm module gaps. ...	63

List of Tables

Table 2-1 Radiometric units.....	14
Table 2-2 Photometric quantities.....	18
Table 2-3 Functions of applied principles.....	24
Table 4-1 Color difference between simulated superposition and measurement.....	39
Table 4-2 Color difference between different considered LEDs and measurement.....	40
Table 4-3 Color difference between two different wavelength LEDs in the same bin.	41
Table 4-4 Built-in color errors by a width of peak wavelength in the same bin.	42
Table 4-5 Color difference between the white boundary and black boundary modules.	42
Table 4-6 Color accuracy of simulation and black / white boundary prototypes.....	44
Table 5-1 Conditions of simulation in LSF approximation method.....	48



Chapter 1

Introduction

During the past several decades, there has been rapid development of displays due to the advanced techniques. Slim format displays can be generally classified to different types basing on radiating methods, which are emissive and passive displays. Emissive displays include the organic light emitting diode (OLED), the plasma display panel (PDP), and the field emitting display (FED)^[1,2,3]. One of the passive displays, liquid crystal display (LCD)^[4], is the most popular slim format display. It should be noted, however, that there have been few attempts to describe a calculation method for the arrangement of color deviation and binned-LEDs, because of the complexities of the conventional ray tracing method. The main purpose of this thesis is to build an efficient calculation system of direct-emitting backlight to analyze the optical properties and color deviation.

1.1 Liquid crystal displays (LCDs)

In liquid crystal displays (LCDs), the liquid crystal (LC) acts as an electro-optic shutter which modulates the amount of incident light. Typical LCD configuration is shown in Fig.1-1, which consists of backlight, polarizer^[5], thin film transistors (TFTs), LC layer, color filters, analyzer, and glass substrates. The backlight system is installed as hindermost device in LCD to provide a planar uniform light source. These may be cold cathode fluorescent lamps (CCFLs)^[6] or light emitting diodes (LEDs)^[7,8,9]. By polarizer absorbing one direction light, the non-polarized light is converted to a linear

polarization. The linear polarized light then propagates through the LC layer, which is placed between two glass substrates (e.g. indium tin oxide, ITO) and driven by a TFT to modulate the linear polarized light rotating angle. According to an absorbed direction of analyzer, the transmission in each pixel of the LCD can be defined as two types, normally white and normally black. The RGB color filter array is fabricated on the top glass substrate to mix the three monochromatic primary colors and produce full color images.

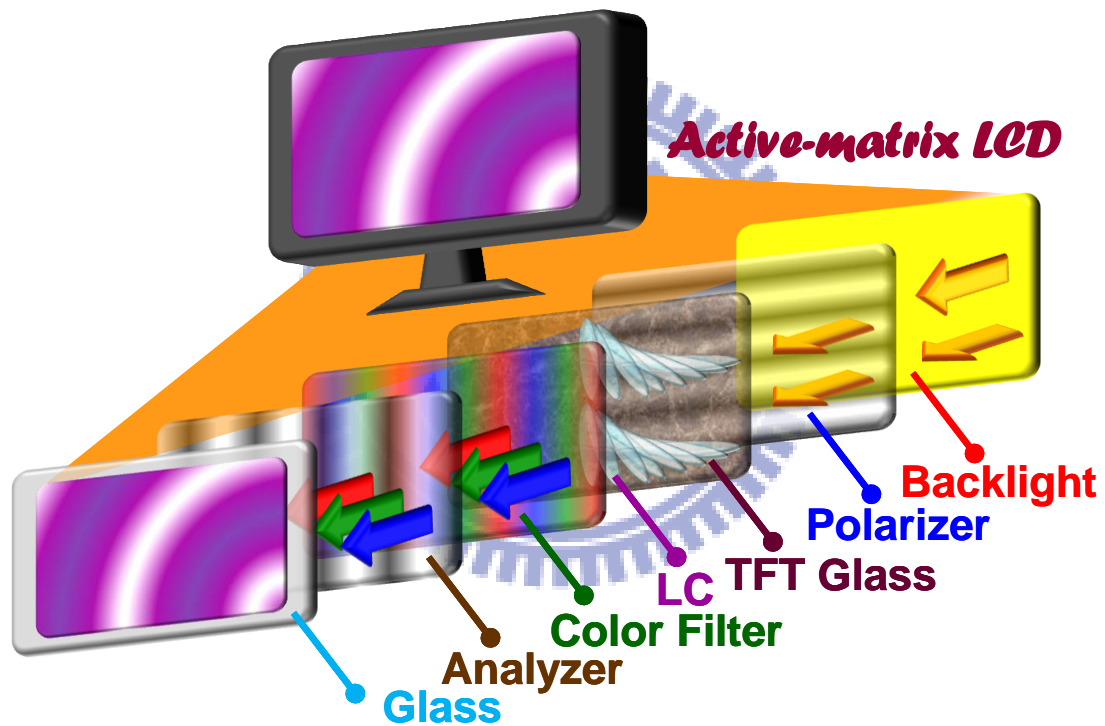


Fig. 1-1 Schematic configuration of a liquid crystal display.

Since the LC panel does not emit light by itself, a backlight system is required to provide illumination. Depending on the position of the light source, the backlight system can be classified into two types generally. One of them is called side-emitting backlight, as shown in Fig. 1-2 (a), when the light source is at the edge of a light guide

plate (LGP). And the other type is called direct-emitting backlight, as shown in Fig. 1-2 (b), when the light source is directly behind the LCD. A side-emitting backlight is typically used in small and middle-sized LCDs because of its small form factor and low power consumption. For example, it usually applied in mobile products since slim thickness and light weight. However, large-sized LCDs are more and more universal around human lives, such as LCD-TVs and electronic billboards. Since a display area is larger, an increased light source is needed to achieve the specified brightness. Compared with an edge-emitting one, direct-emitting LED backlight needs space for mixing light to maintain uniformity and has more benefits, such as application in larger-size LCD, local dimming technology and high-brightness display. Thus direct-emitting backlights are generally applied to large-sized LCDs.

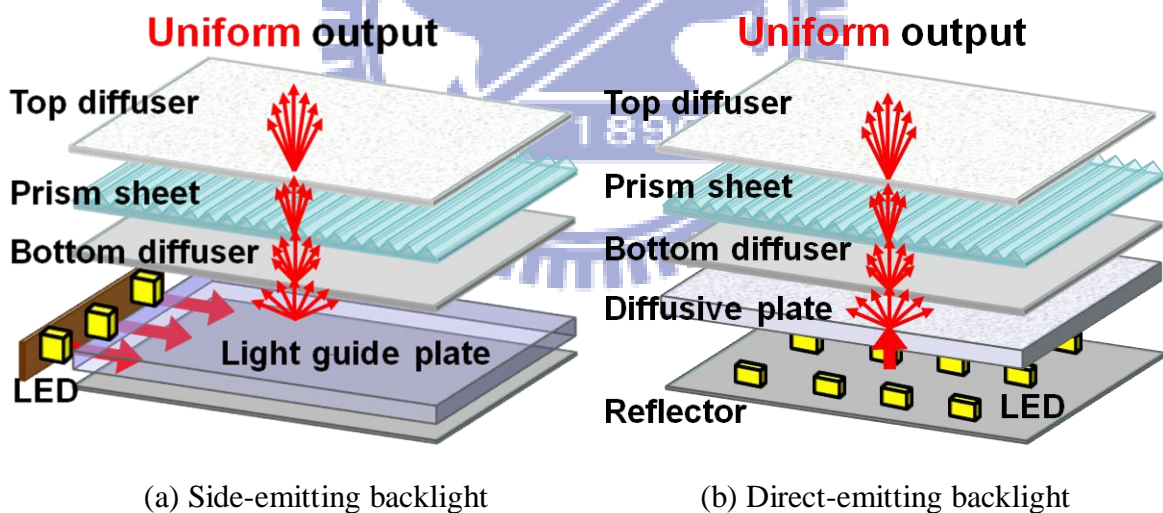


Fig. 1-2 Schematic configuration of the conventional backlight systems.

1.2 Direct-emitting backlight systems

The conventional direct-emitting backlight systems consist of a diffusive plate, optical films, and light sources, as shown in Fig. 1-2. The light sources, which are

CCFL lamps or LEDs, are arranged parallel behind the LC layer, as shown in Fig. 1-3^[10]. A diffusive plate with diffusive particles inside the substrate is laid at a distance, which is called module gap, from the light source. After light is emitted from the light source, it spreads through module gap and diffused by the diffusive plate. The reflector is installed as a light recycle component in the bottom of whole device to reflecting the light which is mirrored by diffusive plate partially. A bottom diffusive sheet, with adjusted scattering ability, is applied to obtain a more uniform light distribution. Then the light propagates into a prism sheet to redirect spreading shape from a large inclined angle in the normal direction. Thus brightness can be enhanced in the normal viewing direction^[11]. Finally, a top diffusive sheet is placed on top of the backlight system, which is applied to protect the micro-structure of the prism sheet and to reduce Moiré patterns^[12]. Then the planar uniform light is outputted from backlight system.

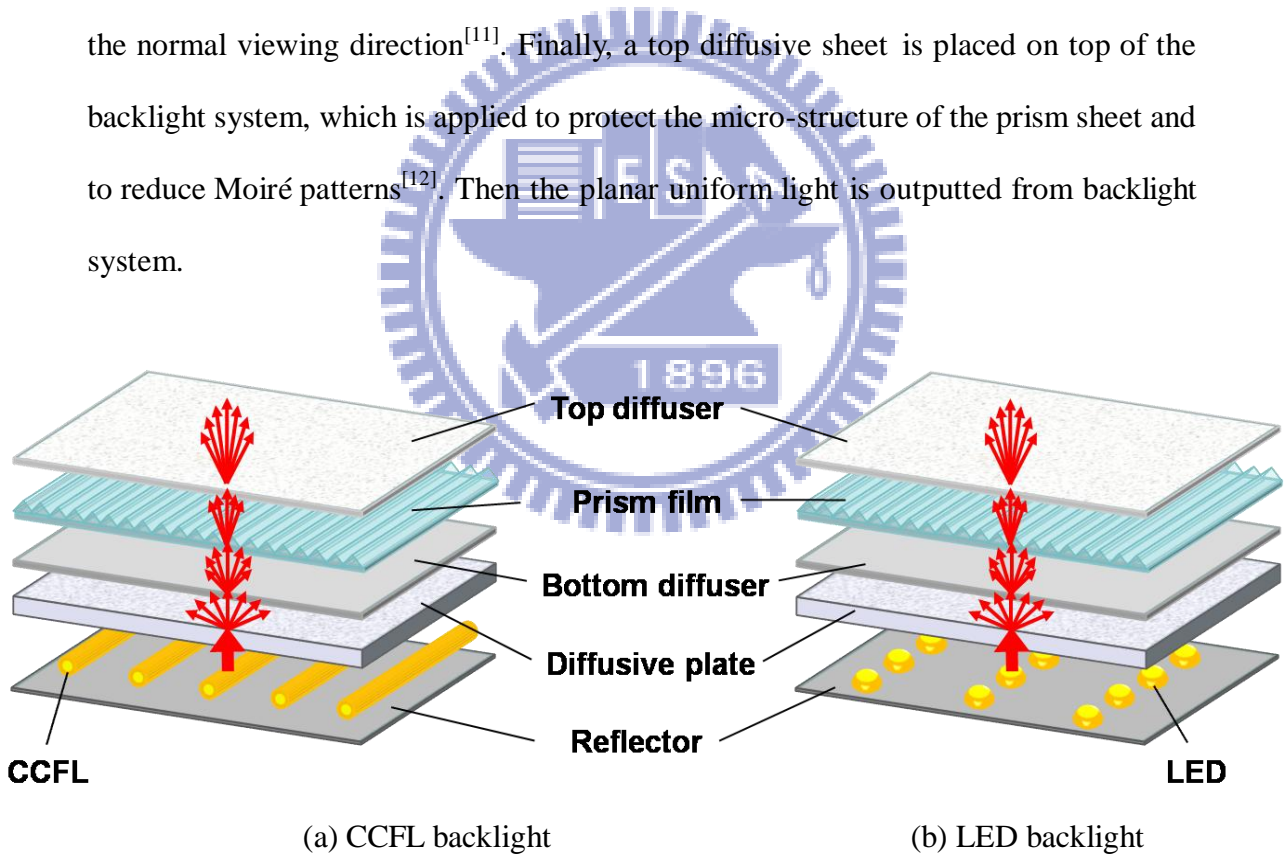


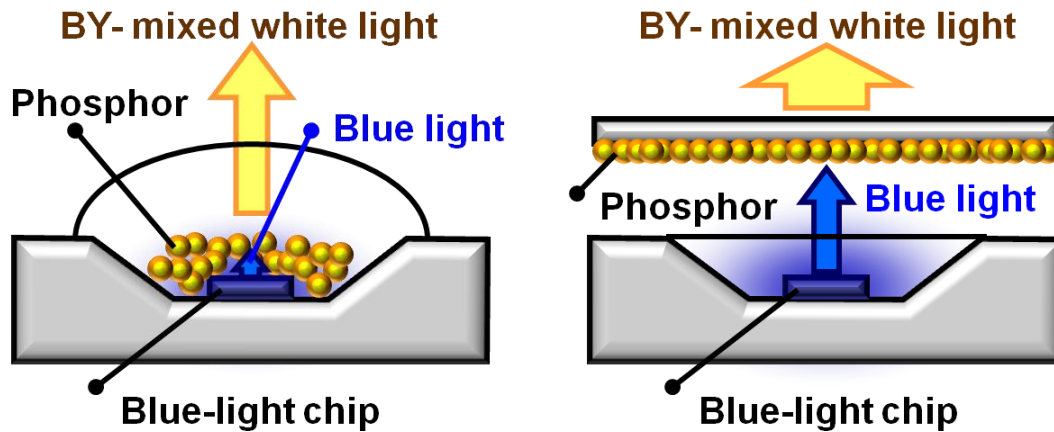
Fig. 1-3 Schematic configuration of the conventional direct-emitting backlight systems.

Additionally, remote phosphor technology applied in backlight system will be introduced in the next section.

1.3 Remote phosphor technology

Remote phosphor technology is extensively applied in white LED illumination. According to its used functions, it can be classified to two applications, point light source and planar light source. In point light source application, remote phosphor technology mainly contributes to increase extraction efficiency and performed higher illuminating brightness when compared with conventional LEDs. In the other application, it mainly contributes to increase uniformity in planar light source.

Remote phosphor technology was firstly developed for LED packaging since Nadarajah's research (2005)^[13]. A light-excited illuminating device configuring with external photo-fluorescent structure is so-called remote phosphor technology. The scheme of the conventional pcLED which utilizes a blue LED chip irradiating Cerium(III)-doped $Y_3Al_5O_{12}$ phosphor^[14] (YAG-phosphor) to obtain white light emission is shown in Fig.1-4(a). The broadband YAG-phosphor is coated on the LED die surface of a blue LED chip and packaged inside the whole device. This configuration has low efficiency because the diffuse phosphor directs 60% of total white light emission back toward the chip and leads losses of energy. Nadarajah *et al.* proposed the scattered photon extraction (SPE) pcLED^[13,15,16,17] which contained a external YAG-phosphor. The external phosphor was coated on an external substrate outside the LED chips as shown in Fig. 1-4(b). Due to the separation of LED die and extraction of backward-emitted rays, the remote phosphor sheet system could convert the point light sources into a planar uniform light source and reduce the backlight thickness. Moreover, the efficiency of SPE pcLED was 61% higher than conventional pcLED.



(a) Conventional pcLED (b) Scattered photon extraction(SPE) pcLED

Fig. 1-4 Scheme configurations of light emitting diodes.

Basing on research of the remote phosphor technology adopted pcLEDs, the direct-emitting backlight with remote phosphor technology is utilized in this thesis. Comparing with conventional direct-emitting backlight, the configuration with large-sized remote phosphor layers coated on flat substrates is shown in Fig.1-5. The phosphor layer is placed between optical films. After light spreading through module gap and diffusing by the diffusive plate, the point light source is converted into planar light source. Then the phosphor layer can be excited by planar blue light and emit yellow light to produce planar white light for backlight. Due to the backward scattering of excited yellow light, the direct-emitting backlight with remote phosphor technology has higher optical efficiency and uniformity than conventional direct-emitting backlight.

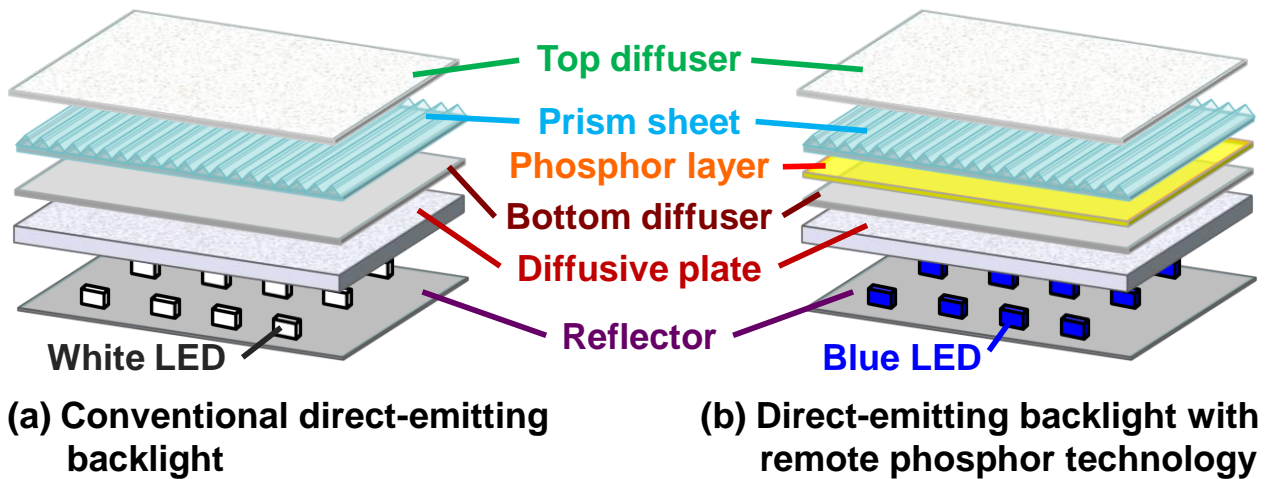


Fig. 1-5 Schematic configuration of (a) conventional direct-emitting backlight and (b) direct-emitting backlight with remote phosphor technology.

1.4 Motivation and objective

Both color uniformity of backlight system and cost down are key issues in LCDs fabrication. Moreover, LED is expected to become the backlight source of next generation, because of enhanced energy efficiency, a larger lifetime, the omission of mercury, and compliance with demand for green technologies. Since the manufacturing effect, LEDs are classified to different bin types by wavelength, brightness and voltage. However, the wavelength requirement of LED is very strict in backlight system. Fig. 1-6 shows a LED binning map^[18], which represents the actual LEDs-bin classified range. From the LED binning map, only the center white bin LED can be chosen as light source in LED direct-emitting backlight. In the other words, the usable LEDs are rare in fabricating for backlight applications.

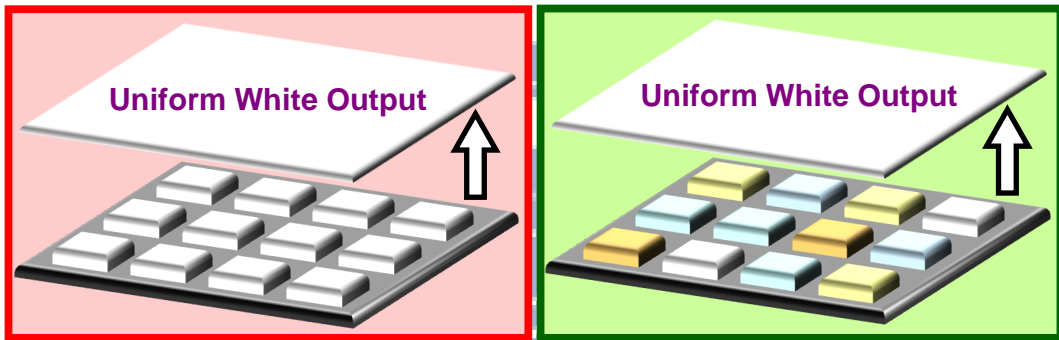
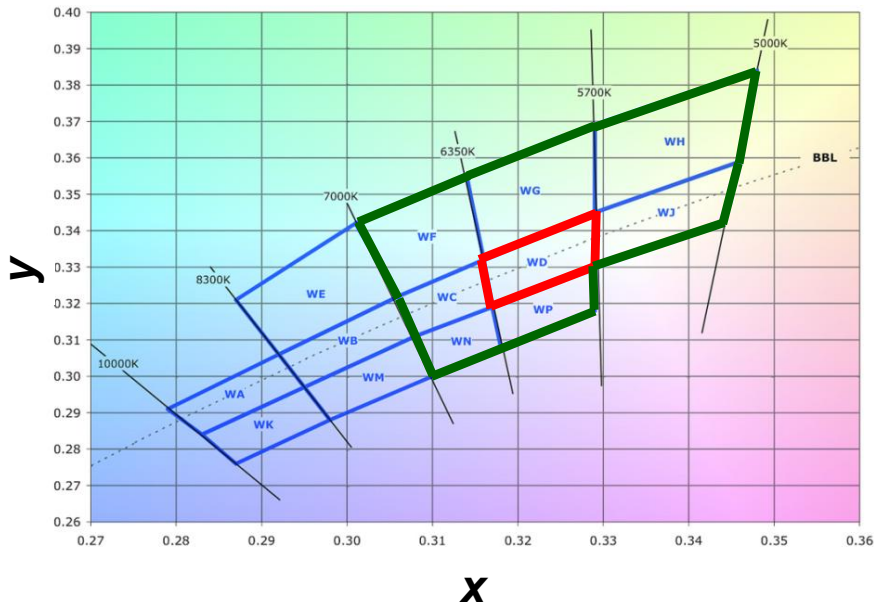
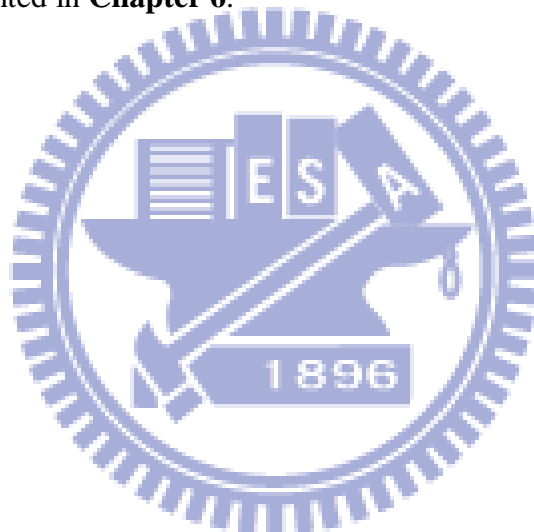


Fig. 1-6 Usable range of LED binning map for application in direct-emitting backlight.

It should be noted, however, that there have been few attempts to describe a calculation method for the arrangement of color deviation and binned-LEDs, because of the complexities of the conventional ray tracing method. The main purpose of this thesis is to build an efficient calculation system of direct-emitting backlight to analyze the optical properties and color deviation. By using the method, whether the phosphor having the wider blue LED binning range and evaluate the binning range under the required chromaticity uniformity or not is verified. According to this calculation system, an optimized binning distribution and arrangement method were proposed. In the last part, by applying the proposed method, the LED binning range for backlight could be extended thus becomes more cost effective.

1.5 Organization of this thesis

This thesis is organized as follows: The principles of backlight systems are presented in **Chapter 2**. In **Chapter 3**, the design concepts and processes of LSF approximation method are described. The simulation results and experimental results to analyze the accuracy of proposed method are verified in **Chapter 4**. In **Chapter 5**, the results of LEDs random arrangement, optimized arrangement, and reducing gap method are discussed. Finally, conclusions of this thesis and recommendations for the future work are presented in **Chapter 6**.



Chapter 2

Light Principles of Backlight Systems

For the purpose of designing and analyzing backlight systems, some optical principles are defined in this chapter. Emitted ray from light source propagates through an optical system, which is usually a homogeneous material, following the linear phenomena of light reacting. Thus geometrical optics is introduced to illustrate the light behavior in backlight systems. Moreover, results of the ray-tracing method can be mainly interpreted by Radiometry and Photometry. Furthermore, basing on the definition of Colorimetry, two color spaces, CIEXYZ and CIELUV, which specify color numerically, are also presented to explain the characterizations of phosphor films in this chapter.

2.1 Geometrical optics in illumination system

By electromagnetic theory and Maxwell equations, light exhibits a phenomenon as electromagnetic waves with time varying electric and magnetic fields when the wavelength of light is much smaller than surrounding objects it propagates through and around. After radiated from a point source, the light waves take a spherical form and travel in all directions. When propagating far away from the source, the light then behave like plane waves. The path of a hypothetical point on the wave front of light is called a ray of light. Thus the behavior of light can be approximated and described by ray optics (geometrical optics), including Snell's law, Fresnel's equation, and other optical principles.

2.1.1 Law of refraction (Snell's law)

Snell's law, also called law of refraction, defines the phenomenon of light refraction in the plane-of-incidence, which consists of an incident ray, a reflected ray, a refracted ray, and a normal direction of the surface. The verification of Snell's law can be proved by Fermat's Principle^[19]. When a light ray having an angle θ_i (the incidence angle) with the surface normal strikes a boundary (interface) of two different optical media, it will induce a refracted ray transmitted through the boundary and makes a new angle θ_t (the refraction angle) with the surface normal, as shown in Fig. 2-1. Based on the definition of Snell's law, the deviation of optical rays due to refraction is defined as the following equation^[20],

$$n_i \sin \theta_i = n_t \sin \theta_t, \quad (2.1)$$

where n_i and n_t are the refractive indices of the incident and transmitting medium, respectively.

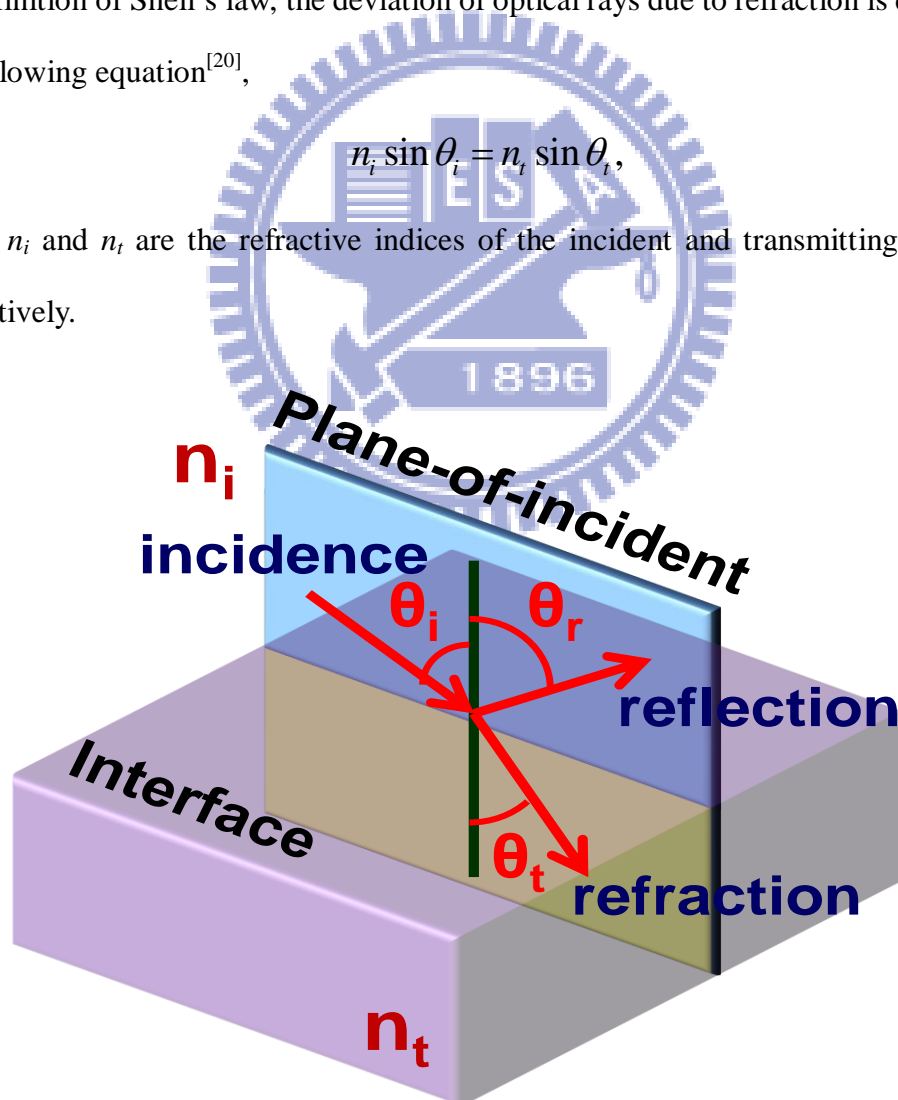


Fig. 2-1 Reflection and Refraction on a boundary surface

2.1.2 Law of reflection

In the plane of incidence, the propagating direction of the reflected rays follows below formula, which is also known as law of reflection^[21]:

$$\theta_i = \theta_r \quad (2-2)$$

where θ_i (incident angle) and θ_r (reflected angle) are the angles of propagation respectively. In other words, the reflected ray and the incident ray propagate with equal but opposite angle in the incident-of-plane of the same media.

2.1.3 Fresnel's equations

Fresnel's equations describe the energy of transmitted and reflected light at an interface between two different optical media. According to the polarization of light, electromagnetic waves can be classified to two types, P polarized light, and S polarized light, which vibrates parallel and perpendicular to the plane of incidence, respectively. The amplitude reflection and transmission coefficients r and t are respectively given by^[22]:

$$r_s = \frac{n_i \cos \theta_i - n_t \cos \theta_t}{n_i \cos \theta_i + n_t \cos \theta_t} \quad (2-3)$$

$$t_s = \frac{2n_i \cos \theta_i}{n_i \cos \theta_i + n_t \cos \theta_t} \quad (2-4)$$

$$r_p = \frac{n_t \cos \theta_i - n_i \cos \theta_t}{n_i \cos \theta_i + n_t \cos \theta_t} \quad (2-5)$$

$$t_p = \frac{2n_i \cos \theta_i}{n_i \cos \theta_i + n_t \cos \theta_t} \quad (2-6)$$

where n_i and n_t are the refractive indices of the incident and transmitting medium, θ_i and θ_t are the angles made by the incident and refracted ray with the surface normal, respectively.

According to radiant flux density (irradiance)^[23], which unit is W/m^2 , the reflectance and the transmittance for polarized light are defined as:

$$R_s = r_s^2 \quad (2-7)$$

$$T_s = 1 - R_s \quad (2-8)$$

$$R_p = r_p^2 \quad (2-9)$$

$$T_p = 1 - R_p \quad (2-10)$$

where R_s and T_s are the reflectances and transmittances for S polarization light, and R_p and T_p are the reflectances and transmittances for P polarization light, respectively. According to the conservation of energy, the reflectance R and transmittance T of a random polarized light (eg. the nature light) striking the interface can be defined as the average of the polarized case as following equations:

$$R = \frac{R_s + R_p}{2} \quad (2-11)$$

$$T = \frac{T_s + T_p}{2} \quad (2-12)$$

Basing on laws of reflection and refraction, the behaviors of light, reflected, and refracted, could be described by geometrical optics. Besides, by Fresnel's equations, the reflectances and transmittances at an interface of two media could be calculated. Thus the energy of a particular light on the defined receiver could be obtained.

Therefore, the propagating direction of a light ray in an optical system can be traced and simulated to design and optimize the optical performances of the backlight

systems.

2.2 Radiometry

Radiometry is the science of measurement in electromagnetic radiation. It can gauge optical radiation within wavelengths ranging from 10 nm to 10^6 nm^[24]. Consequently, the light source, which using ultraviolet-, visible-, and infrared-light, in optical systems can be analyzed by radiometry. Radiometric quantities include radiant energy, radiant flux, radiant intensity, irradiance, radiant exitance, and radiance. These fundamental quantities which characterize the energy content of radiation are used in SI unit^[25] and summarized in Table 2-1.

Table 2-1 Radiometric units.

Quantity	Symbol	Definition	Unit
Radiant energy	Q		joule
Radiant flux	Φ	dQ/dt	watt
Radiant intensity	I	d Φ /d Ω	watt/sr
Irradiance	E	d Φ /dA	watt/m ²
Radiant exitance	M	d Φ /dA	watt/m ²
Radiance	L	d ² Φ /dA _⊥ d Ω	watt/(m ² · sr)

(t: time, Ω : solid angle, A: area)

Radiant energy Q is the energy of a collection of photons (as in a laser plus). According to quantum mechanics, which classified by Albert Einstein, the energy of a single photon is $h\nu$. Radiant flux Φ is defined as the measure of total power of radiation,

which is the total emitted from a light source or the total debarcation on a particular surface. Basing on radiant energy Q and radiant flux Φ , the other quantities are obtained by various geometric normalizations.

Radiant intensity I is generally used to describe the characteristics of sources whose size is infinitesimal, such as a point source. The definition of I is the radiant flux Φ emitted per unit of solid angle Ω in a given direction of a specified surface, which the propagating radiation is incident passing through or upon, as shown in Fig.2-2 (a).

Irradiance E clarifies radiation distribution on a received plane. The definition is the radiant flux per unit area A of a specified surface, which the spreading radiation is incident on or passing though, as shown in Fig. 2-2 (b).

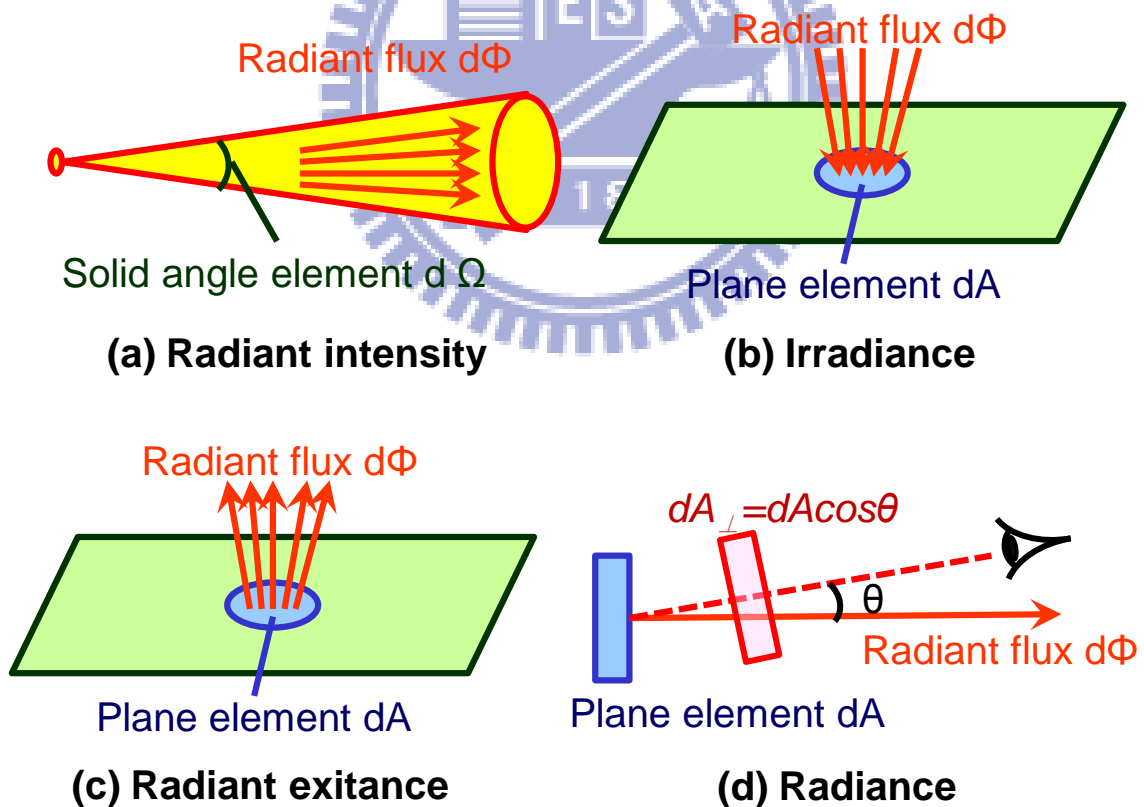


Fig. 2-2 Defining geometry of radiometric quantities.

When the radiant flux leaving the plane per unit area A is considered, the term radiant exitance M is used instead of irradiance E . But the defined in the formulas are expressed by the same equation. Radiant exitance M clarifies radiation distribution on the plane which emits the radiation, as shown in Fig. 2-2 (c).

If an extended source, such as a planar source, is considered, radiance L is used to describe its characteristic. The definition of radiance L is the radiant flux Φ per unit project area A_{\perp} and per unit solid angle Ω of a specified surface, which the propagating radiation is incident on or passing through, as shown in Fig. 2-2 (d). The projected area of the plane element equals to $dA\cos\theta$, where θ is the angle between the normal of the plane element and the direction of observation.

2.3 Photometry

Compared to Radiometry that describes all radiant energy, Photometry considers the responses to the optical radiation of human visual system, which are sensitivity at all wavelengths of visible light. Photometric quantity is an operationally defined quantity designed to represent the way in which the human visual system evaluates the corresponding radiometric quantity. The radiant power at each wavelength is weighted by CIE luminous efficiency curve, and the standard model that represents response or sensation of brightness for the eye versus wavelength is reproduced in Fig. 2-3. In particular, the optical radiation within the wavelengths range between 380 nm and 780 nm called visible light are discussed by photometry.

Photometric quantities include luminous energy, luminous flux, luminous intensity, illuminance, luminous exitance, and luminance. The definitions of photometric quantities are related to the corresponding radiometric quantities through the luminous

efficiency curve. The photometric quantities whose unit is based on lumen (lm)^[25] are shown in Table 2-2. The unit lumen is defined as ‘luminous flux emitted into a solid angle of one steradian by a point source whose intensity is 1/60 of the intensity of 1 cm² of a blackbody at the temperature of platinum (2042K) under a pressure of one atmosphere.’

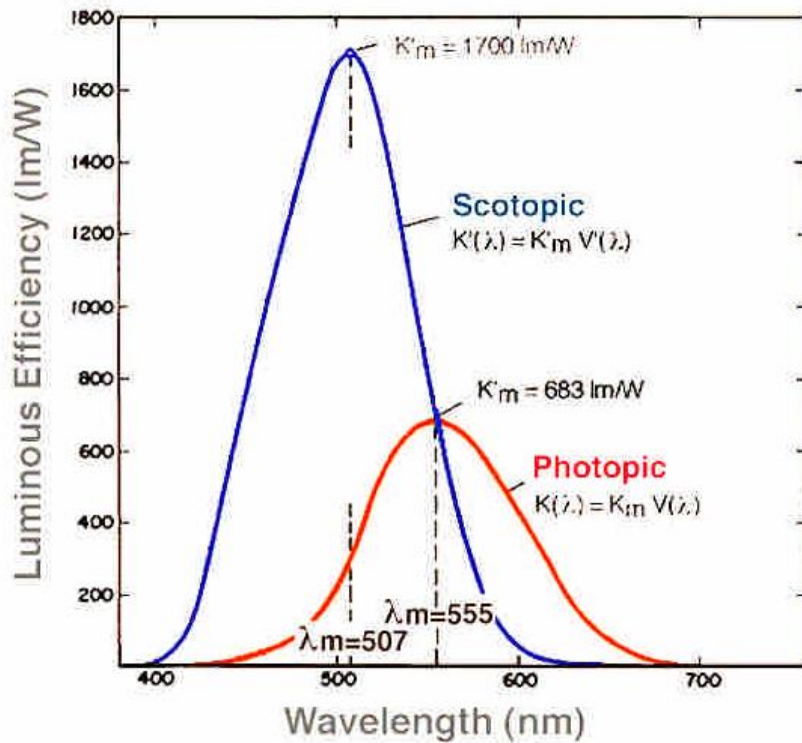


Fig. 2-3 Scotopic and Photopic spectral sensitivities.

From the definition of lumen, the corresponding maximum spectral efficiency of human eyes, which one watt is equal to 680 lumens, is at the wavelength 555 nm. Thus, the luminous flux Φ_v emitted from a source with a radiant flux $\Phi_\lambda(\lambda)$ is given by:

$$\Phi_v(\lambda) = 683 \text{ lm/w} \cdot \int V_\lambda(\lambda) \Phi_\lambda(\lambda) d\lambda \quad (2.3)$$

where λ is the wavelength and $\int V_\lambda(\lambda)$ is the normalized luminous efficiency function depicted in Fig. 2-4^[26].

Table 2-2 Photometric quantities.

Quantity	Symbol	Definition	Unit
Luminous energy	Q_v		lumen · s
Luminous flux	Φ_v	dQ_v/dt	lumen(lm)
Luminous intensity	I_v	$d\Phi_v/d\Omega$	lumen/sr or candela
Illuminance	E_v	$d\Phi_v/dA$	lumen/m ² or lux
Luminous exitance	M_v	$d\Phi_v/dA$	lumen/m ²
Luminance	L_v	$d^2\Phi_v/dA_{\perp}d\Omega$	lumen/(m ² · sr) or nits

(t: time, Ω : solid angle, A: area)

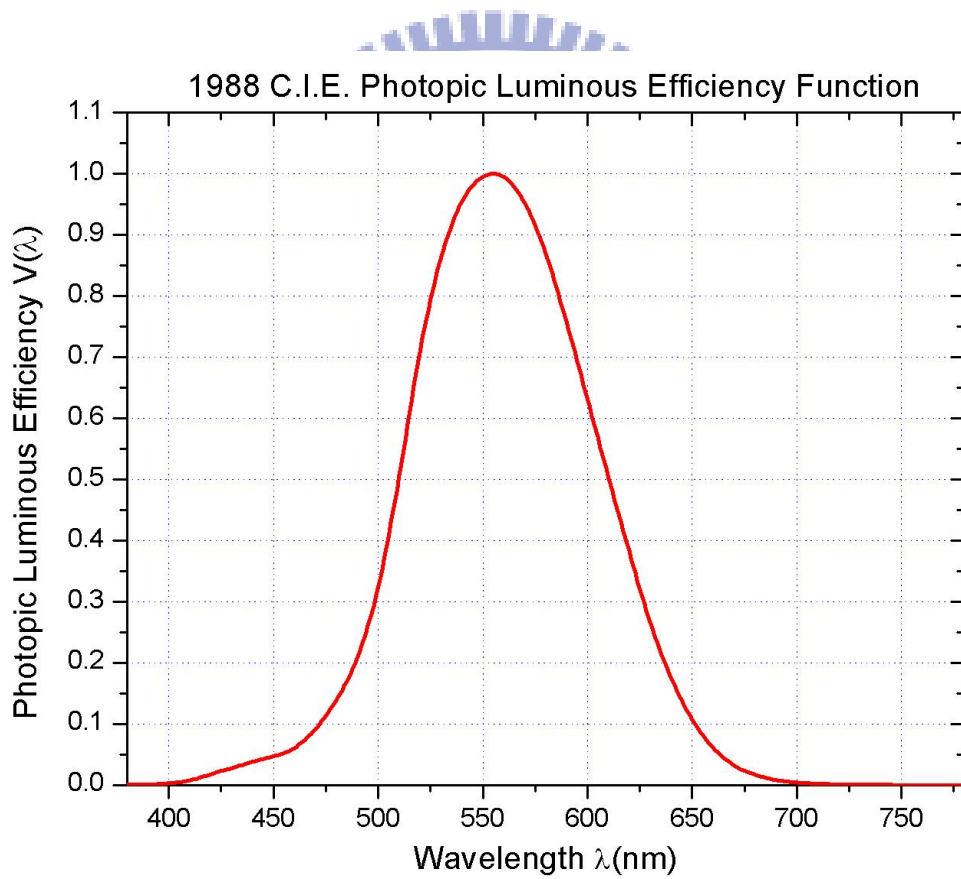


Fig. 2-4 1988 CIE Photopic Luminous Efficiency Function

2.4 Colorimetry

Colorimetry is the science designing and quantifying color comparison and matching in human eyes. As mentioned in prior paragraph, the photometric quantities have provided measures to describe the amount of energy for visible light, where the optical radiations within wavelengths range from 380 nm to 780 nm. However, in human visual system, the optical radiations stimulate not only intensity response (brightness) but also chromatic response (chromaticity). In human eyes, the retina contains two major types of light-sensitive photoreceptor cells used for vision: the rods and the cones, which are responsible for low-light monochrome vision and for color vision, respectively. Therefore, colorimetry is imported to specify the chromatic performance of backlight units in this thesis. The CIE 1931 xyY and CIE 1976 LUV color spaces, which have been developed for denoting colors numerically, are described in the following paragraphs.

2.4.1 CIE 1931 XYZ color space

The CIE 1931 XYZ system, created by the International Commission on Illuminance (CIE, Commission internationale de l'éclairage) in 1931, is one of the first mathematically defined color systems that quantify colors numerically^[27]. The human eye has three types of cones that perceive for short (S), middle (M), and long (L) wavelengths light, often referred to as red, green, and blue, respectively. Accordingly, in definition, three parameters are used to describe a color sensation. The tristimulus values of a color are the amounts of three primary colors in a three-component additive color model, which is needed to match that test color^[28]. In the CIE 1931 XYZ system, the tristimulus values are called X, Y, and Z. The tristimulus values for a color with a

stimulus $\Psi(\lambda)$ can be evaluated from the color matching functions, the numerical illustration of the chromatic response of standard observer^[29] (see Fig. 2-5), according to the following equations:

$$X = k \int_{vis} \Psi(\lambda) \bar{x}(\lambda) d\lambda \quad (2.4)$$

$$Y = k \int_{vis} \Psi(\lambda) \bar{y}(\lambda) d\lambda \quad (2.5)$$

$$Z = k \int_{vis} \Psi(\lambda) \bar{z}(\lambda) d\lambda \quad (2.6)$$

where k is a constant and the integral is taken in the visible light wavelength. The $\bar{y}(\lambda)$ is set in order to identify the value the same as the spectral luminous efficiency function $V_\lambda(\lambda)$ mentioned earlier. Thus the tristimulus value Y directly expresses a photometric quantity.

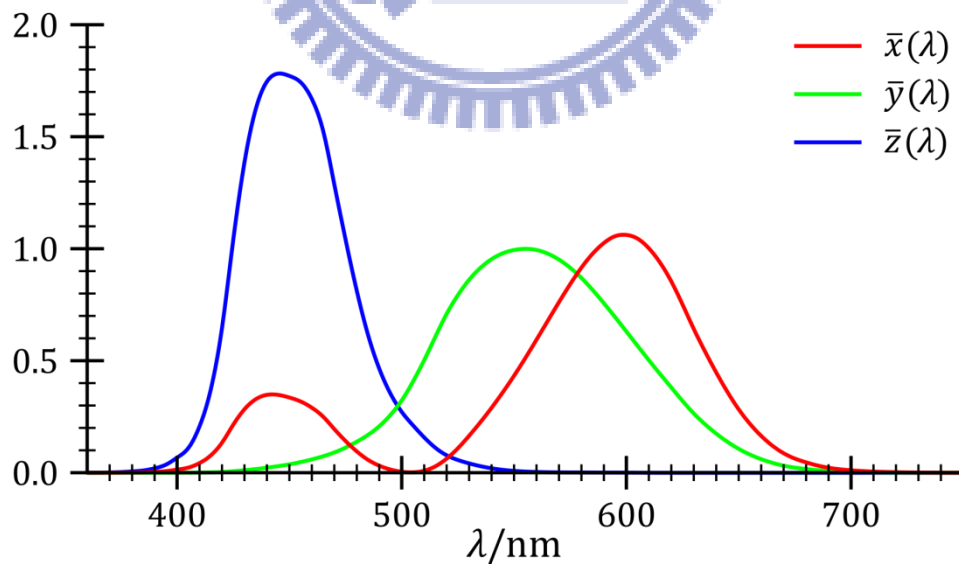


Fig. 2-5 Color matching functions $\bar{x}(\lambda)$, $\bar{y}(\lambda)$, and $\bar{z}(\lambda)$ in the CIE XYZ color system.

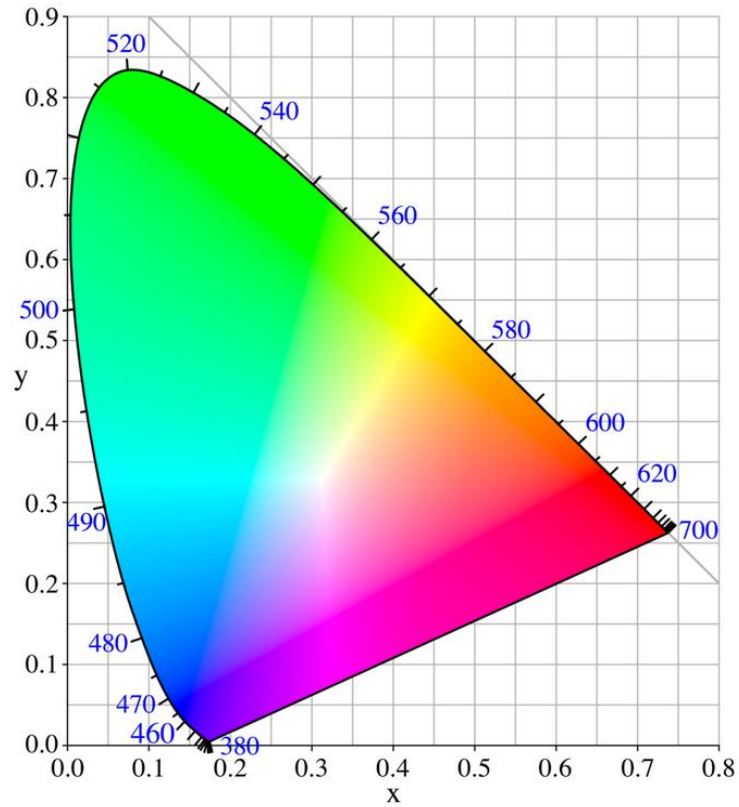


Fig. 2-6 xy chromaticity diagram of CIE XYZ color system.

Basing on CIE 1931 XYZ system, a color could be represented by applying the tristimulus values X , Y , and Z in a three-dimensional color space, called CIE 1931 XYZ color space. Besides, for convenient descriptions of colors, a color space represented by x , y , and Y , known as CIE 1931 xyY color space, was evaluated^[30]. In this color space, the x and y are defined as following equations:

$$x = \frac{X}{X + Y + Z} \quad (2.7)$$

$$y = \frac{Y}{X + Y + Z} \quad (2.8)$$

$$z = \frac{Z}{X + Y + Z} = 1 - x - y \quad (2.9)$$

where z coordinate could be neglected by providing Y parameter which is a measured value of the luminance of a color. Therefore, the chromaticity description of a color could be expressed more conveniently in a two-dimensional plane, which is called CIE xy chromaticity diagram and be widely used in custom (see Fig. 2-6).

However, the xy chromaticity diagram is highly non-uniform and has been found to be a serious problem in custom^[31]. The color difference between two colors could not be calculated by using CIE 1931 XYZ color space or xy chromaticity diagram. Therefore, a uniform color space, the CIE 1976 LUV color space, is proposed to replace the non-uniform CIE 1931 XYZ color space.

2.4.2 CIE 1976 LUV color space

The CIE 1976 LUV color space proposed by CIE in 1976, which is an approach to define an encoding with uniformity in the perceptibility of color difference^[32]. This uniform color space is based on a simple-to-compute transformation of the CIE 1931 XYZ color space^[33,34]. For the non-linear relations from CIE 1931 XYZ color space to CIE 1976 LUV color space, the three-dimensional orthogonal coordinates adopted in CIE 1976 LUV color space are defined as follows^[35]:

$$L^* = 116(Y / Y_n)^{1/3} - 16 \quad (2.10)$$

$$u^* = 13L^* (u' - u_n') \quad (2.11)$$

$$v^* = 13L^* (v' - v_n') \quad (2.12)$$

where u' and v' is the coordinates of two-dimensional $u'v'$ chromaticity diagram (see Fig. 2-7), which is used similarly to xy chromaticity diagram, defined as Equation 2.13 and 2.14. Y_n , u_n' , and v_n' are the tristimulus value and the chromaticity coordinates u'

and v' of reference white, respectively.

$$u' = \frac{4X}{4X + 15Y + 3Z} \quad (2.13)$$

$$v' = \frac{9Y}{X + 15Y + 3Z} \quad (2.14)$$

Basing on the uniform CIE 1976 LUV color space, the color difference of two colors could be calculated simply and directly without changing based domain. The color difference $u'v'$ between two colors (u_1', v_1') and (u_2', v_2') at the $u'v'$ chromaticity diagram is defined as^[36]:

$$\Delta u'v' = \sqrt{(\Delta u')^2 + (\Delta v')^2} = \sqrt{(u_1' - u_2')^2 + (v_1' - v_2')^2} \quad (2.15)$$

In this thesis, Equation 2.15 is imported to judge the chromatic performance of the backlight units.

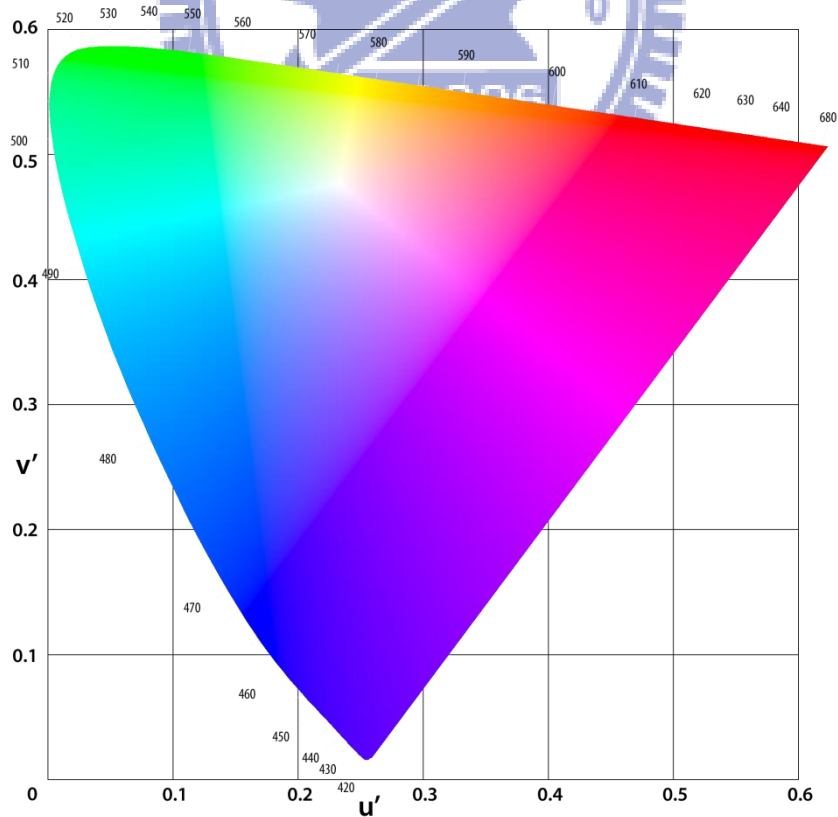


Fig. 2-7 $u'v'$ chromaticity diagram of the CIE LUV color system.

2.5 Summary

Table 2-3 summarizes the principles mentioned earlier in this chapter. In this thesis, ray-tracing method was used to explain properties of light spread function (LSF). By Snell's law, law of reflection, and Fresnel's equations, the propagation trajectory and the carried energy of light could be calculated. Besides, basing on radiometry and photometry, the wavelength-corresponded spectrums with different detected locations of backlight illustrated the compositions of emitted (blue) and stimulated (yellow) light. Furthermore, the flux and chromaticity distribution of the backlight can be simulated by the numerical superposition in commercial calculated software, MATLAB. Accordingly, the CIELUV color space and the color difference $\Delta u'v'$ were utilized to judge the optical performances of the backlight units, which are the most important part for developing simulation models of backlight system. Therefore, the measurement framework will be discussed in the following chapter.

Table 2-3 Functions of applied principles.

Method	Principle	Function
Ray tracing	Snell's law	Calculating propagation trajectory and carried energy of light.
	Law of reflection	
	Fresnel's equations	
Radiometry & Photometry	Light flux properties	Characterizing light scattering properties of phosphor films.
	Photopic spectral sensitivity	
Colorimetry	CIE LUV color space	Specifying chromaticity performance of backlight output distribution.
	Color difference ($\Delta u'v'$)	

Chapter 3

Concept of LSF Approximation Method

The purpose of this thesis is to extend the blue LED binning range for remote phosphor backlight system. The first step is to build an accurate calculation model for the system. Here the chromaticity and luminance uniformity of the phosphor can be effectively calculated by the spectral distributions of the different binned LEDs under the considered configuration. As the structural parameters, including the pitch, gap, and optical films, are defined, the light spreading function (*LSF*) by single LED is measured first. Therefore, we can calculate the chromaticity distribution of the backlight by the numerical superposition of the LSF against the conventional ray-tracing computation.

3.1 LSF approximation method

The LSF approximation method was built to analyze the optical property and color uniformity of backlight system before manufactured process in a factory. Here the procedures of calculated method could be summarized to the flowchart in Fig. 3-1. Based on the calculation of LSF approximation method, a color deviation of a backlight could be computed and controlled less than the required light flux and chromaticity uniformity by choosing acceptable binning ranges, which are defined by wavelength, flux, and V_f . Moreover, by designing and optimizing binning distribution and arrangement, the more outer binned-type and binned-ratio of LEDs could be chosen to use in LCD backlights. In other words, according to this calculation system, the LEDs information of a good enough color uniformity backlight, which $\Delta u'v'$ less

than an acceptable value of color deviation, were evaluated by the simulation.

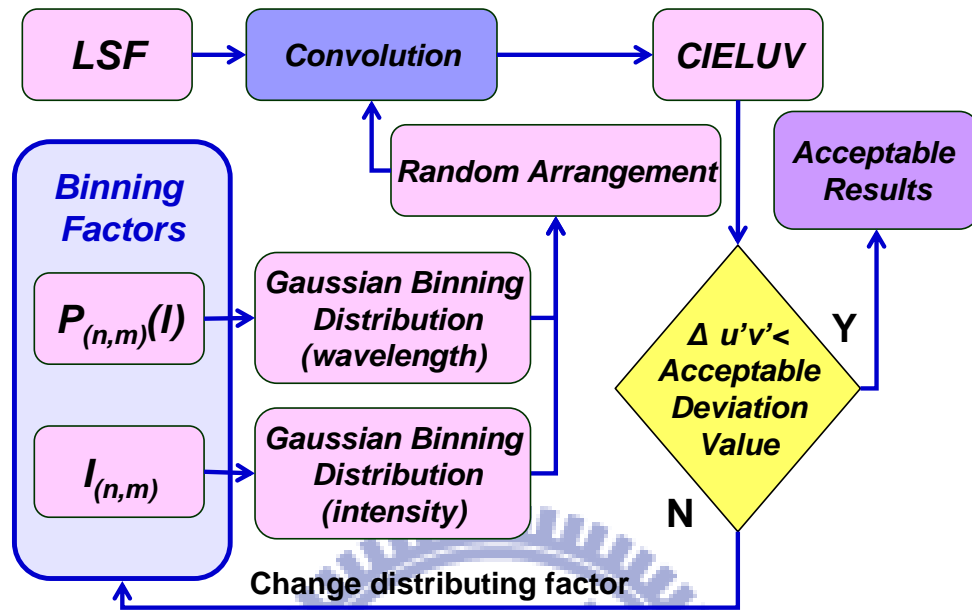


Fig. 3-1 Calculation model flowchart of backlight chromaticity.

3.1.1 Light spread function (LSF)

The first step of the procedure was to measure the light spread function (LSF)^[37] of the backlight system module under single LED illuminating. The measurement setup was shown as Fig. 3-2. Since the LSF would be changed with the varying LED, module gap and optical films, the parameters should be defined before measuring it. Therefore, the measured LSF completely characterized the parameters of the backlight system configuration.

In a case of this thesis analyzing, the gap of module is 30 millimeter, and the encapsulation style of LED, whose driving voltage is about 3.2 V, is a bare chip made by Everlight Electronics CO., LTD. Besides, the optical films from bottom to top are diffuser plate, phosphor sheet, which is also called PEBBLE made by Sony CO.,

diffuser sheet, BEF and DBEF, sequentially. Under these conditions, the LSF of single LED (Fig. 3-3) was measured by CCD camera (ProMetric 1603F-1)^[38], as shown in Fig. 3-4. Since the LSFs are similar under the same encapsulation style of LED and module structure, this step of procedure could be just measured once, and the result indicates to represent LSF of every LED. According to the measured data of LSF, a intensity affected weight of LED in every backlight location could be obtained, and the flux uniformity of backlight system can be superposed. Furthermore, considering the difference of color composition in varied binned-LEDs, the color deviation of backlight system could be calculated, which are described in the following paragraphs.

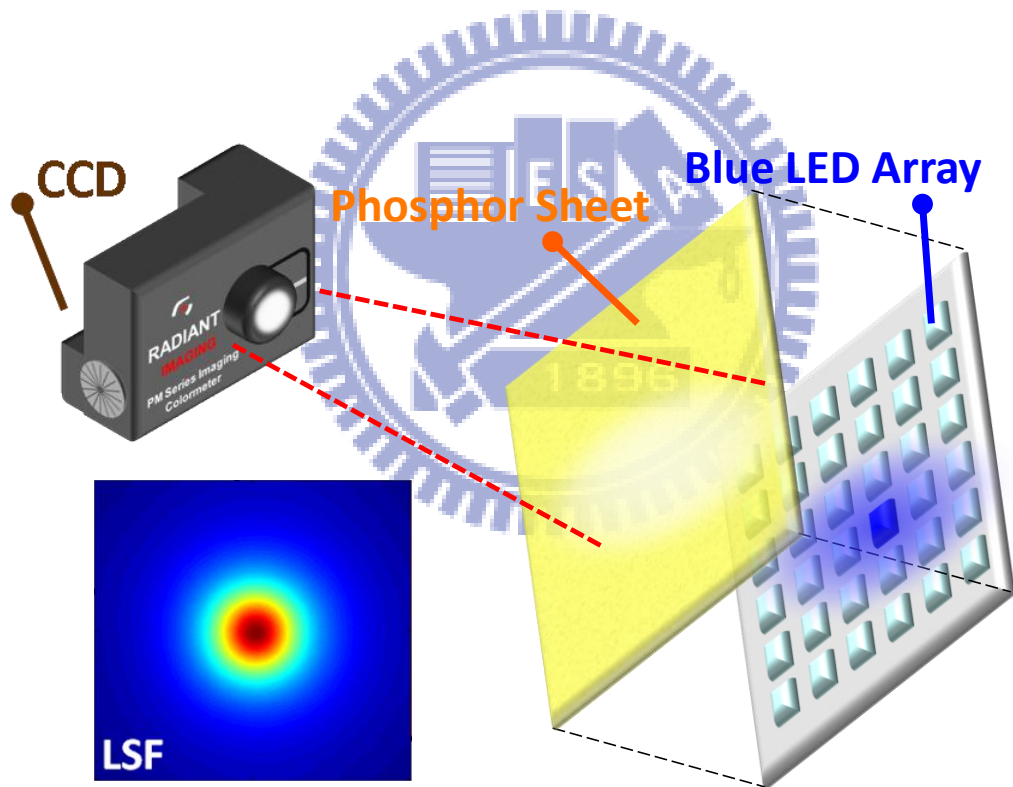


Fig. 3-2 Measurement setup of light spread function.

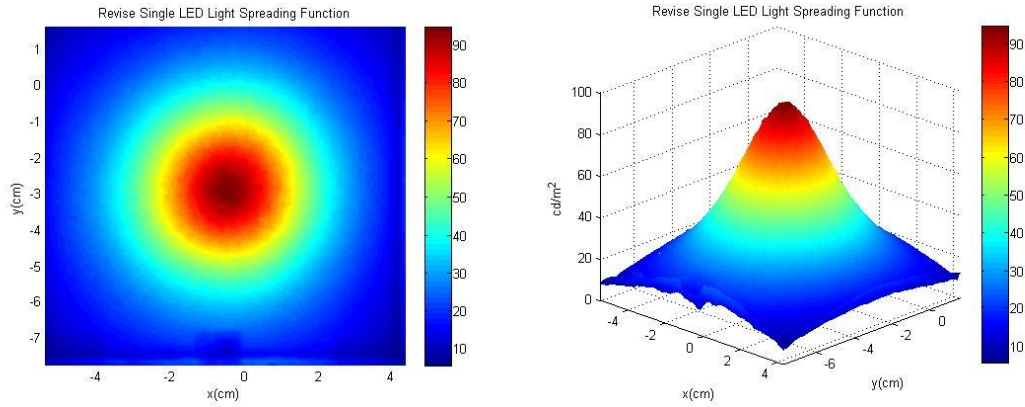


Fig. 3-3 Light spread function of single LED illumination with phosphor.



Fig. 3-4 CCD camera (ProMetric 1603F-1).

3.1.2 Binning factors and spectrums

After the LSF measurement, the spectral distribution of the various binned LEDs with the considered phosphor film would be measured. Fig. 3-5 illustrates the measurement setup. The spectral distributions were varied with the different binned LEDs, so the relative spectrums^[39] represented the binning factors.

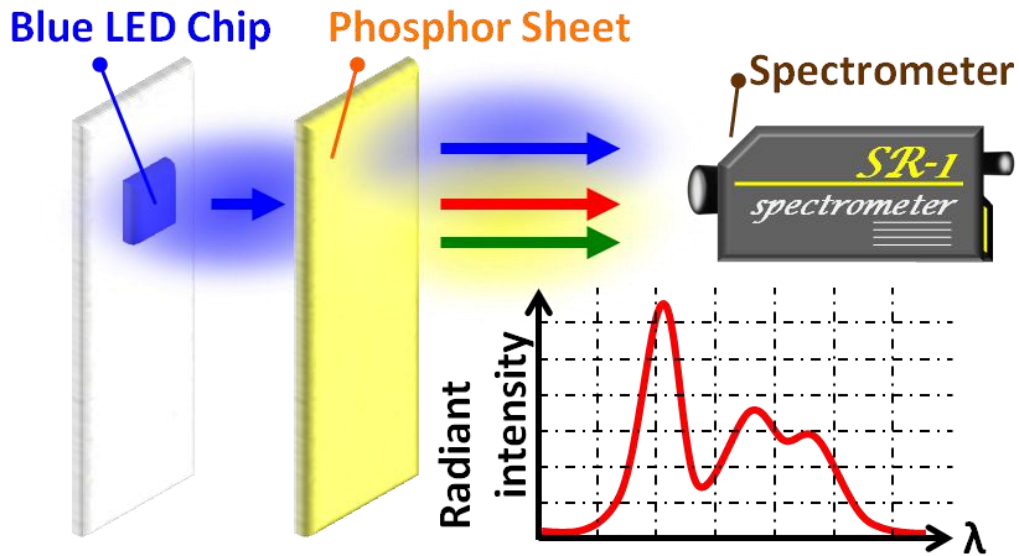


Fig. 3-5 Spectral measurement of binned LED with phosphor film.

It is worth noting that the spectral radiance has varied composition on different locations and viewing angles. It's caused from the diverse angular radiance distributions of the excitation and emission light. The phosphor-scattered blue light has higher directivity than the phosphor-emitted yellow light, so there is the color dispersion pattern of measured LSF, as shown in Fig. 3-6.

In this section, spectrums measured by spectrometer (Topcon SR-UL1R^[40], see Fig. 3-7) are shown in Fig. 3-8 and Fig. 3-9 with the same conditions in the prior LSF section. According to principles of remote phosphor technology, a spectrum could be analyzed and classified to two parts: one is short wavelength range, which composing the blue light emitted by LED, and the other is long wavelength range, which consisting of yellow light stimulated by phosphor sheet.

Fig. 3-7 shows measured spectrums with the same LED and phosphor sheet in the different locations of backlight system. By normalizing the maximum intensity of spectrums, when a distance with the location above LED is farther, the intensity ratio

of yellow light divided by blue light in spectral configuration is higher. This phenomenon occurs by different field shapes of emitted blue light and stimulated yellow light. Since field shapes of blue light and yellow light are directional and lambertian, respectively, the blue component is higher than yellow one in normal detection, as mentioned in the previous paragraph.

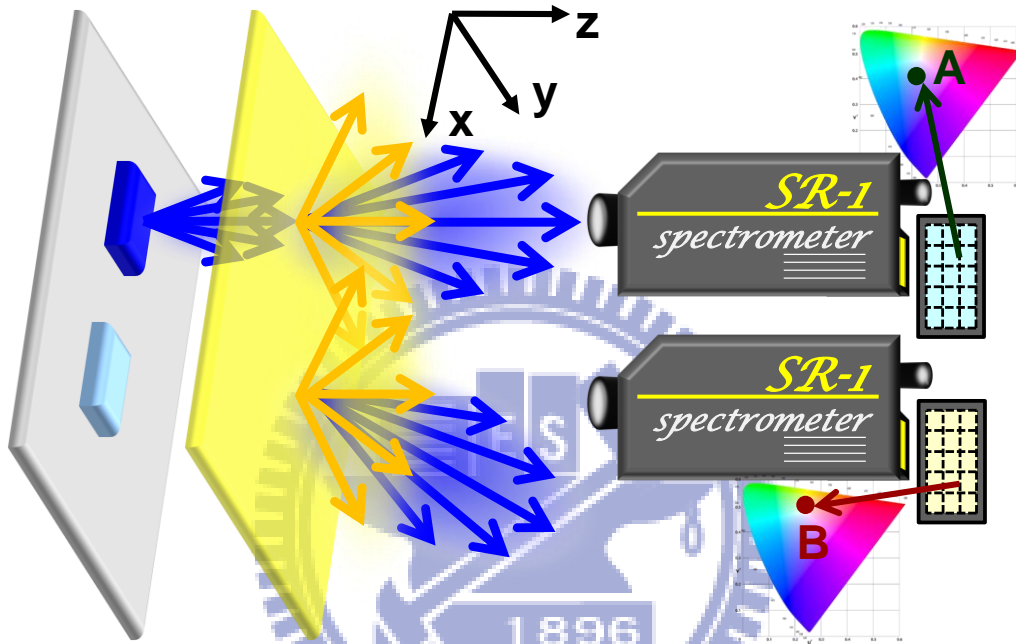


Fig. 3-6 Different composed blue and yellow light in different locations.



Fig. 3-7 Spectrometer (Topcon SR-UL1R).

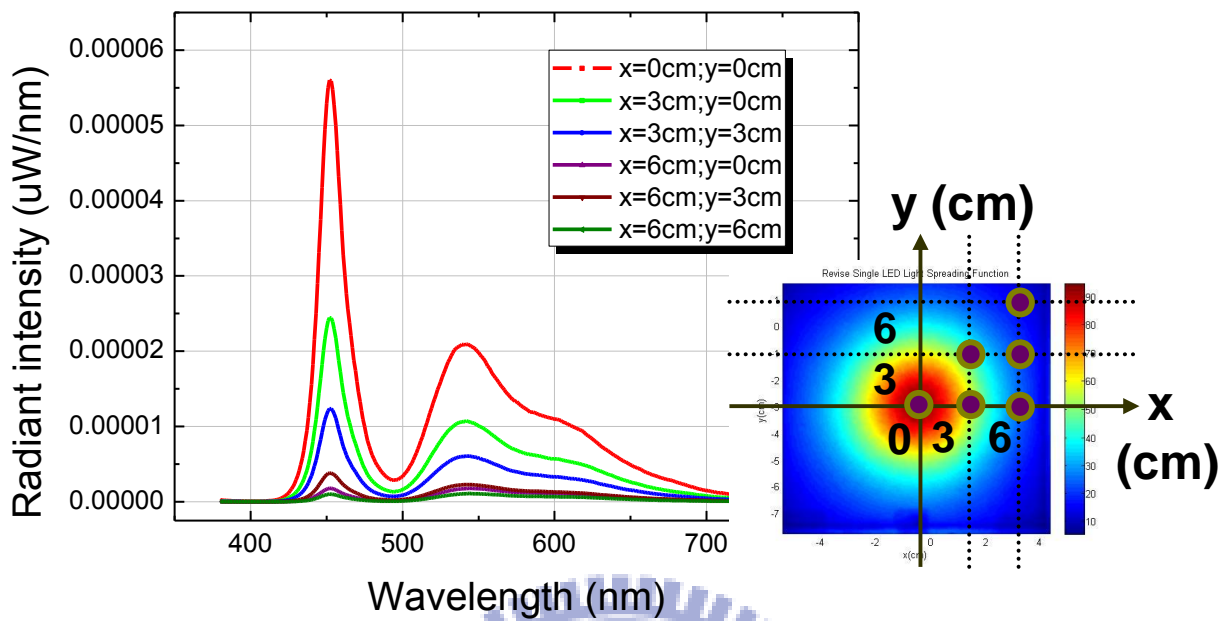


Fig. 3-8 Spectrums of blue LED with remote phosphor in different locations.

The normalized spectrums of various binned-LEDs with a phosphor sheet are shown in Fig. 3-9. Comparing different curves of this picture, the compositions of blue emitted light in spectrums are just shifted by each other, and the flux shapes of yellow stimulated light are almost the same but have different intensity maxima, which can be explained by phosphor emission and excitation data, as shown in Fig. 3-10. Based on phosphor materials, a phosphor sheet composed red and green stimulated light^[41], which is made by Sony CO., is chosen for the better color rendering index. The dashed lines indicate the phosphor sheet absorptive ability in different wavelengths of blue LEDs, which is proportional to the maximal excitations of red and green light. Besides, the solid lines illustrate the spectral distribution of red and green emissive light.

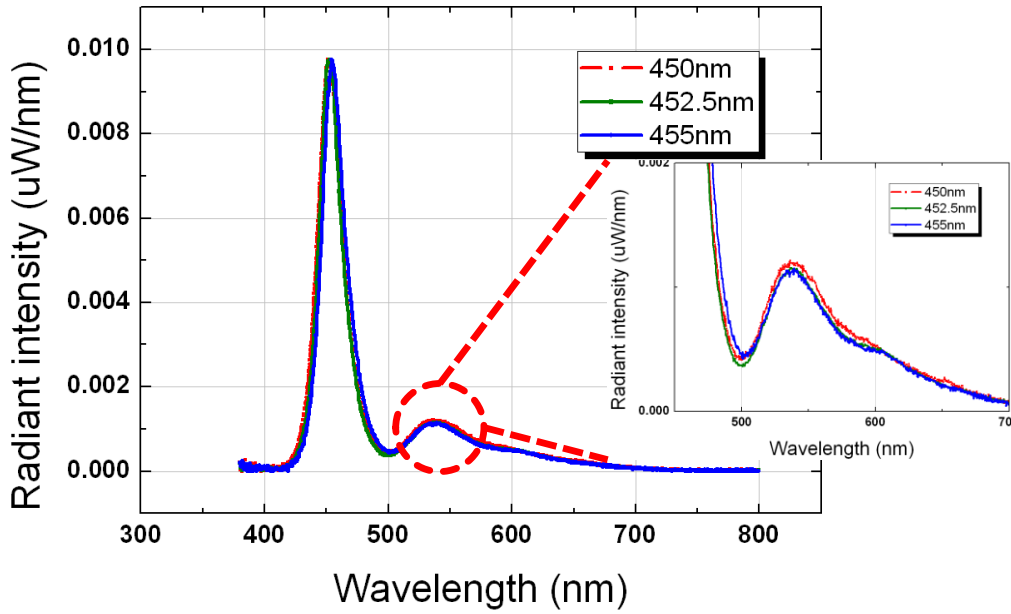


Fig. 3-9 Spectrums of various binned-LEDs with remote phosphor.

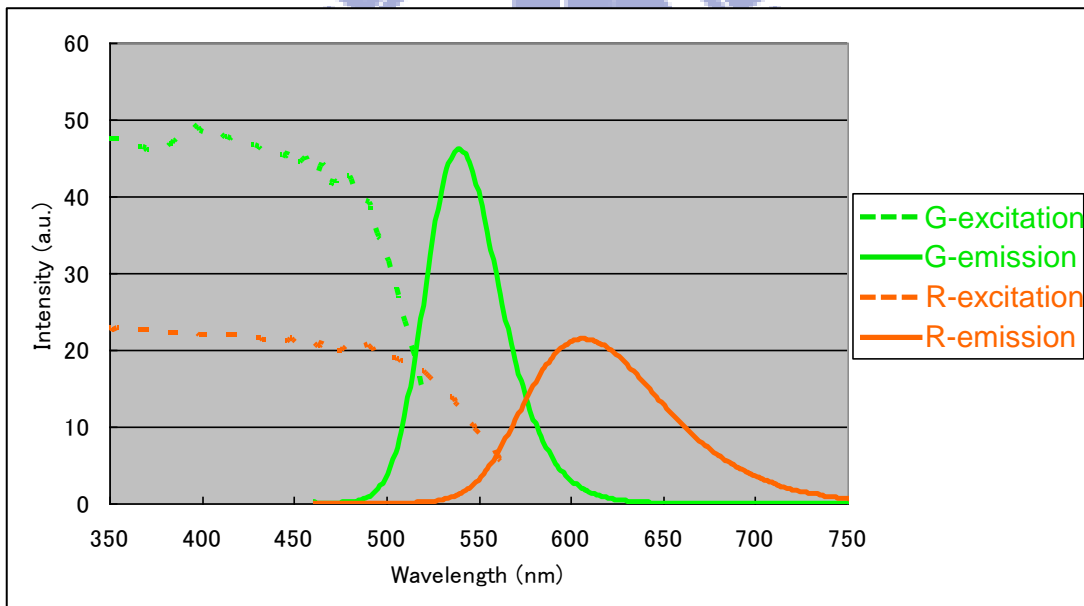


Fig. 3-10 Phosphor emission and excitation data.

3.1.3 Gaussian binning distribution

The effect of chromaticity uniformity in the backlight system would be strongly affected by the LED binning distribution, which be sorted by wavelength and flux. In Fig. 3-11 (a) and (b), the discrete curve represents the practical wavelength bin

distribution, including 0th, ±1st and ±2nd bin types. This discrete distribution is described by the applied Gaussian function^[42],

$$R(\lambda) = \frac{1}{\sigma \times (2\pi)^{0.5}} \times \exp\left(-\frac{(\lambda - \lambda_0)^2}{2 \times \sigma^2}\right), \quad (3.1)$$

where $R(\lambda)$ is bin distribution sorted by wavelength λ . The λ_0 symbol defines the peaked wavelength in the standard bin. And the waist of the Gaussian function σ indicates the width of this bin distribution. Since the Gaussian function, $R(\lambda)$, is continuous, it should be convolution with the comb function to transform into the discrete one, and be multiplication with the rectangular function to limit the range width of bins,

$$R'(n) = \left[R(\lambda) * \sum_{n=-\infty}^{+\infty} \delta(\lambda - n \cdot \Delta) \right] \times \text{rect}\left(\frac{n}{N \times \Delta}\right). \quad (3.2)$$

Where $R'(\lambda)$ could be simply characterized the amount ratio in the different binned-LEDs. The n and N are the order and total of bin types, and Δ indicates the wavelength width range of single bin. Moreover, the bin sorted by flux is also characterized by the same process.

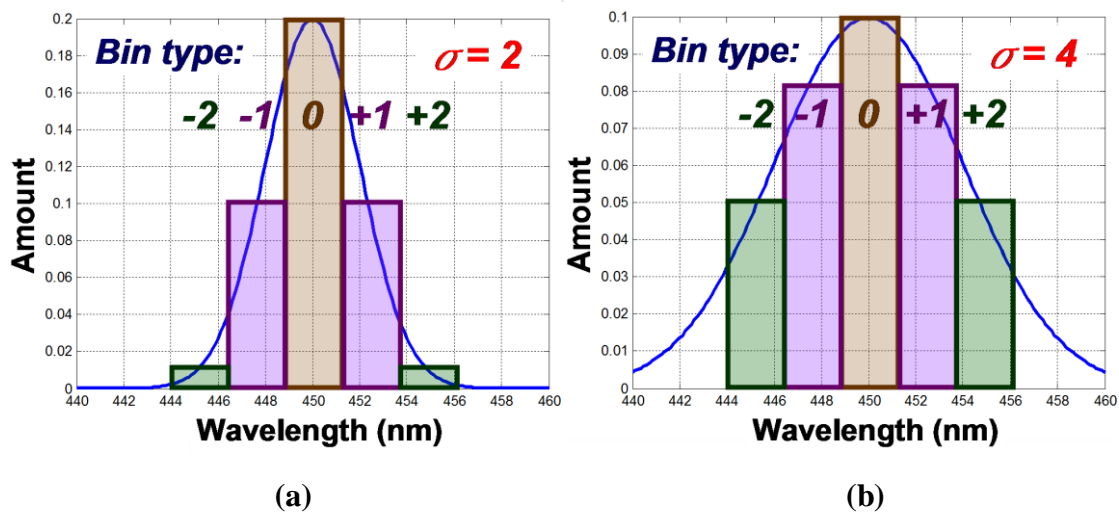


Fig. 3-11 Gaussian function with the waist (a) $\sigma=2$; (b) $\sigma=4$, and the ordinals of each bin.

3.1.4 Convolution

Basing on the normalized LSF, the luminance distribution of the LED array with phosphor would be summed by the superposition,

$$L(x, y, \lambda) = \sum_s \sum_t \left[LSF(x, y) * \left(L_{(s,t)} \cdot P_{(s,t)}(\lambda) \cdot \delta(x - sp_x, y - tp_y) \right) \right], \quad (3.3)$$

where the weights $P_{(s,t)}$ and $I_{(s,t)}$ of the sampling function $\delta(x - sp_x, y - tp_y)$ are the spectral binning factors (normalized spectral distribution) and flux binning factors (maximum luminance of the LSF obtained from binned LED) varied with the LED position (s, t) . The spectral radiance distribution at any point (x, y) on the phosphor emission surface could be obtained by this function, which is defined as spatially spectral distribution.

3.1.5 Comparing results

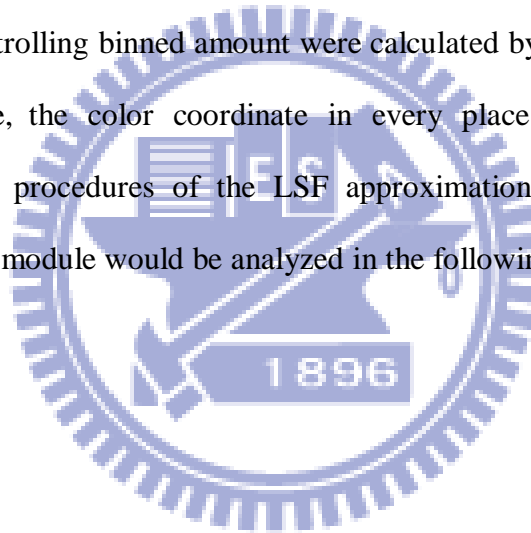
The chromaticity distribution of the backlight system module at the considered position could be transformed from the spatially spectral distribution function by the definition of the CIELUV color space. The evaluating factor is defined as

$$\Delta_{(s,t)} = \sqrt{(u'(x_s, y_t) - u'_e)^2 + (v'(x_s, y_t) - v'_e)^2}, \quad (3.4)$$

where the (s, t) indicates the position exactly above the LED at the s -th line and t -th row. Here the data were compared with the expected value. One set of the calculated results would be verified with the experimental measurement of a small-size prototype.

3.2 Summary

To develop a simulation model to test color deviation of backlight system and design an acceptable binned distribution, the backlight configurations, which were integrated a direct-emitting backlight with the remote phosphor technology, were first specified. In the LSF approximation method, a CCD camera measured LSF completely characterized the conditions of LED encapsulation style, module gap and optical films. Moreover, the spectral distribution of the various binned LEDs with the considered phosphor film was measured by spectrometer. Combing the radiant distribution of LSF and the binning factors of spectrum, the chromaticity distribution of backlight with controlling binned amount were calculated by commercial software, MATLAB. Therefore, the color coordinate in every place of backlight can be simulated simply by procedures of the LSF approximation method. Further, the accuracy of proposed module would be analyzed in the following chapter.



Chapter 4

Verification

In this thesis, the remote phosphor sheet direct-emitting backlight system was chosen as the analyzed structure. According to the procedures of LSF approximation method mentioned in previous chapter, the color deviation of backlight system, which could be evaluated by software simulating, is the key issue of this thesis. Thus, the accuracy of proposed method is very important and would be analyzed in this chapter.

4.1 Accuracy of LSF approximation method

To evaluate the direct-emitting backlight with a specific LED binning distribution, the commercially mathematical software was utilized to accomplish this purpose. In the software, the remote phosphor sheet direct-emitting backlight system was set up as shown in Fig. 4-1, which composed of blue LED chips, reflector white, diffuser plate, phosphor sheet, diffuser sheet, BEF and DBEF. In the simulation, the module gap (h) and the period of blue LED chips (p) were both 30 mm. The range of blue LED peak wavelengths in the center bin (0^{th}) was from 455.0 nm to 457.5 nm, and the others were every 2.5 nm nearby the center one. Besides, in the same conditions, a small-sized remote phosphor sheet direct-emitting backlight system (180 mm x 180 mm x 30 mm) with 36 blue LED chips (6 x 6) was demonstrated to verify the calculation model, as shown in Fig. 4-2 (a) and (b). According to the target of the thesis, the acceptable color deviation of whole backlight was 0.014. This required condition was strict, so the accuracy of computation was very important. In this section, the errors between

simulation and measurement were discussed step by step.

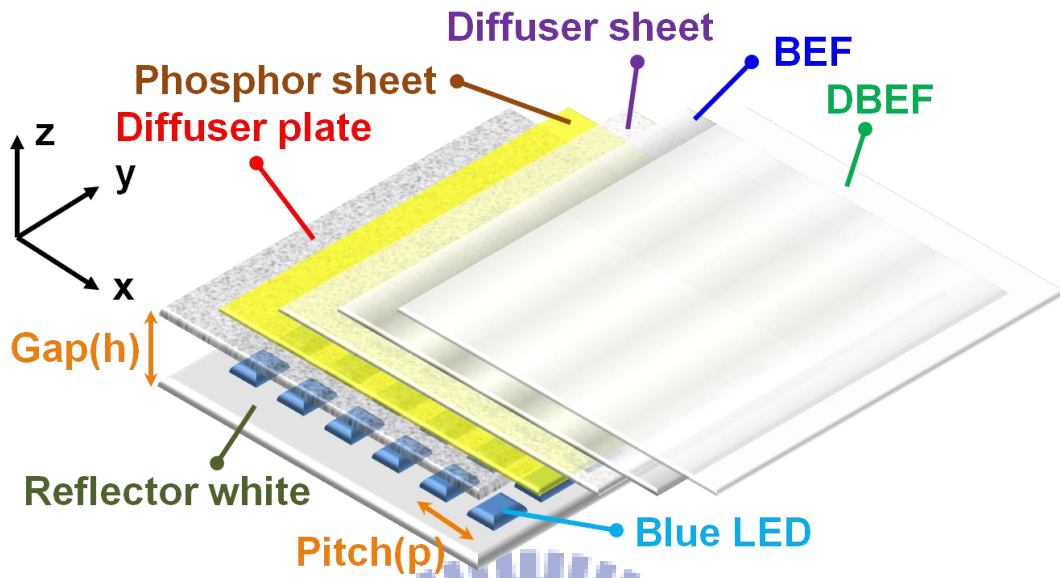


Fig. 4-1 Structures of simulated remote phosphor direct-emitting backlight model.

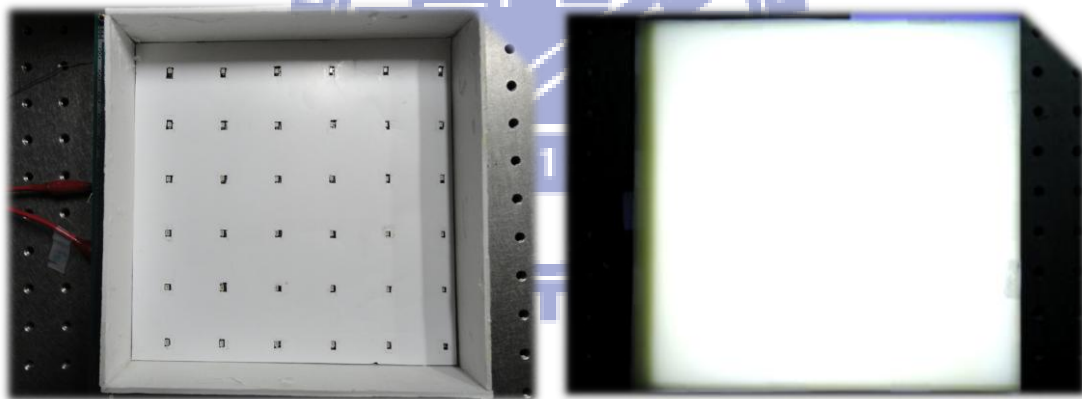


Fig. 4-2 Ten inch direct-emitting prototype of (a) blue LEDs; and (b) phosphor sheet and optical films with LED illuminating.

4.1.1 Correctness of LSF superposition method

The first step is to exam the correctness of the proposed LSF superposition method.

Fig. 4-3 (a) shows the experiment setup for verification. Considering the 3×3 LED

array, the calculation result is derive from the superposition of the nine LSF, as shown in Fig. 4-4. From Table 4-1, the color difference between measurement and calculation is 0.0007. The errors are caused from the limitation of the spectrometer dynamic range. Here the electronic noise and straight light strongly affect the spectrum distribution of the superposition.

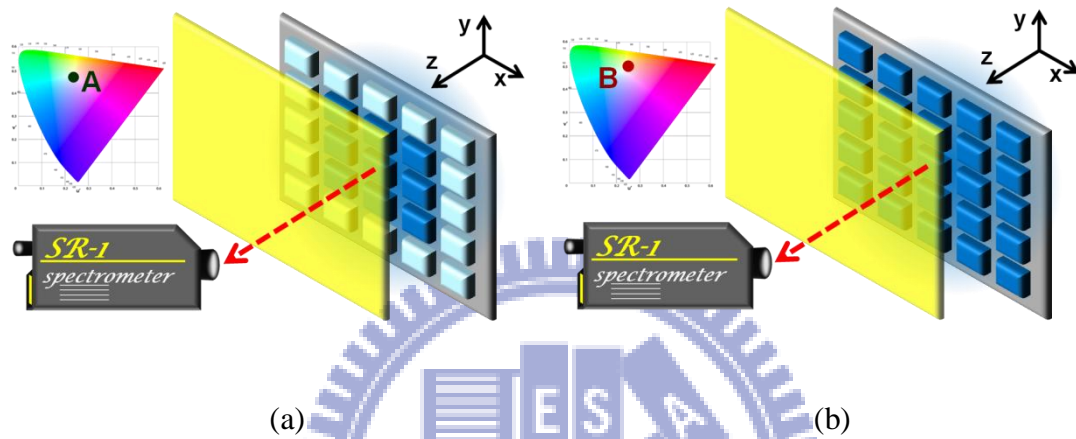


Fig. 4-3 Spectrums measurement setup with turning on (a) 3×3 LEDs; and (b) 5×5 LEDs.

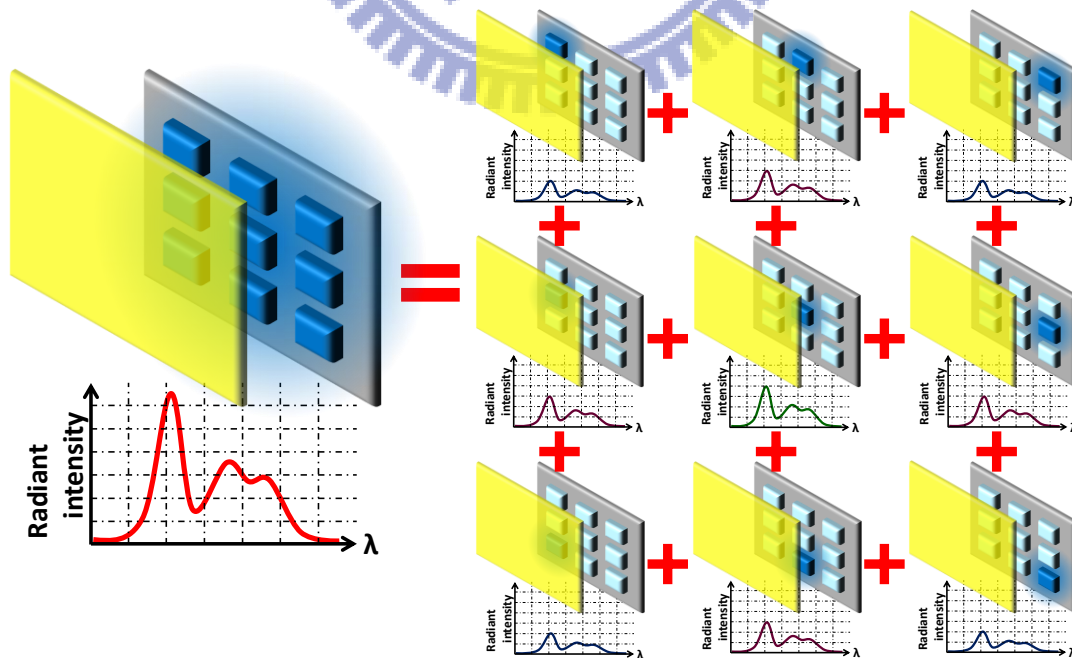



Fig. 4-4 Simulated spectrums superposition compared with measurement data.

Table 4-1 Color difference between simulated superposition and measurement.

Color Coordinates In Center Place 	
Measurement (3×3)	0.1905,0.4560
Calculation (3×3)	0.1908,0.4554
Difference	0.0007

4.1.2 Tolerance of self-fabricated module

Second, we found out the tolerance of the measurement set up. The deviation between different times measurement is 0.0012. There are two main reasons. One is the unstable of the self-fabricated module, and the small tilt angle (θ) between the panel normal and the axis of objective, as shown in Fig. 4-5. The other is the radiance tolerance of the instrument, where the noise rises as the increased exposure time.

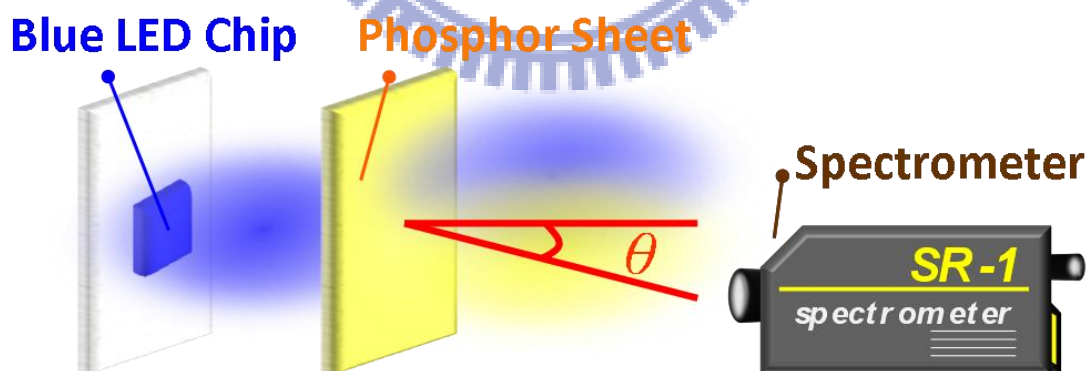


Fig. 4-5 Measurement deviation by small tilt angle between panel normal and detector.

4.1.3 Affected color composition range of LED

Thirdly, we compared the measured 5×5 and 6×6 data with the calculated 3×3 result to verify the approximation of 3×3 LSF superposition. We assume the LEDs of outer ring from 3×3 matrix wouldn't affect the color composition in the center. The comparisons are shown in Table 4-2. Here the color difference is 0.0071 and 0.0130 respectively. The huge deviation shows that the 3×3 assumption is incomplete for this case. However, the calculated 5×5 case has small color difference from the measurement results. Therefore, the 5×5 approximation is more suitable to simulation the color deviation.

Table 4-2 Color difference between different considered LEDs and measurement.

Color Differences ($\Delta u'v'$)	Measurement (5×5)	Measurement (6×6)
	0.1915,0.4625	0.1908,0.4554
Calculation (3×3)	0.0071	0.0130
0.1908,0.4554		
Calculation (5×5)	0.0006	0.0060
0.1921,0.4623		

4.1.4 Built-in tolerance from bin width

The fourth step is to examine the calculation tolerance caused from bin width. We consider the situation that the 457.7 nm and 460.0 nm blue LEDs are all in 457.5~460.0 nm bin. The color difference between them by measuring 3×3 LEDs is 0.0034, as shown in Table 4-3.

Table 4-3 Color difference between two different wavelength LEDs in the same bin.

Peak wavelength (nm)	Color coordinate (u'v')
457.7	0.1901,0.4604
460.0	0.1887,0.4635
Difference	0.0034
Difference (intensity variable $\pm 5\%$)	0.0043

The real manufacture of 3×3 single bin LEDs, which composing varied peak wavelengths, was constructed for testing the built-in error, as shown in Fig. 4-6. The color coordinates measured from module is compared with the simulated condition, which LEDs peak wavelengths are all in the bin edge, as compared in Table 4-4.

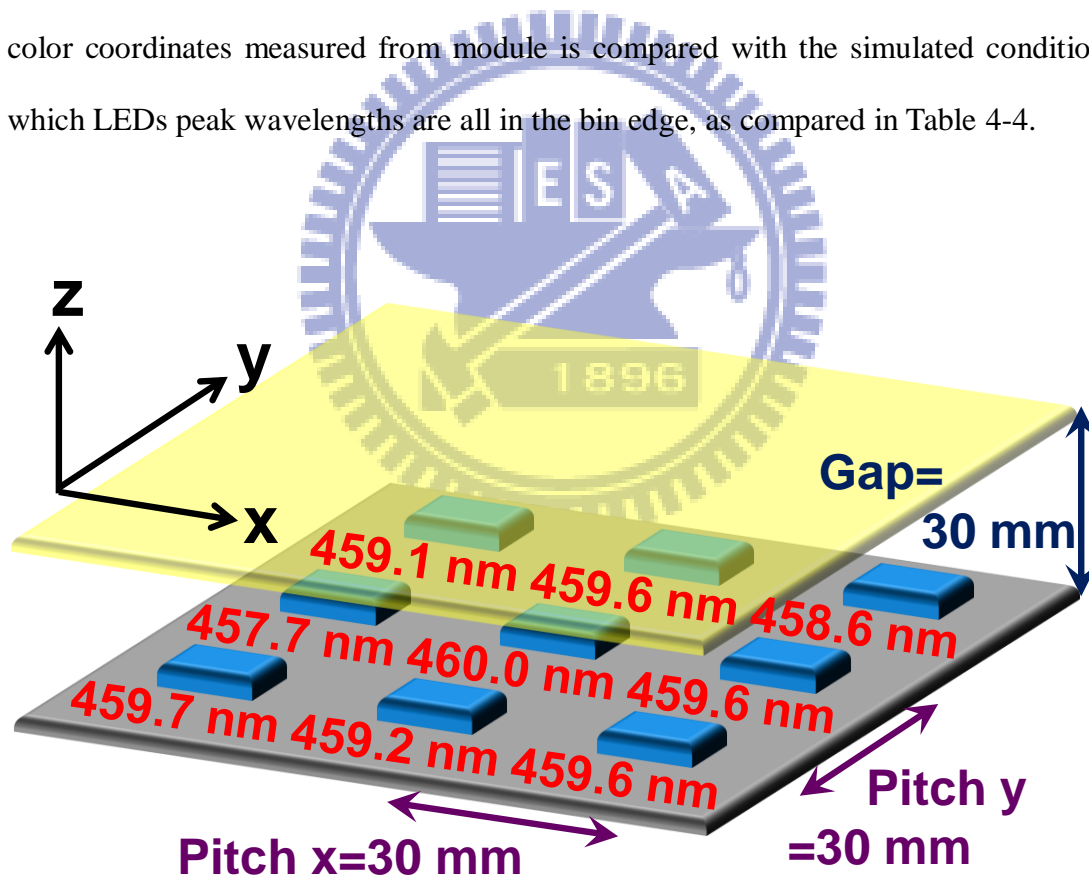


Fig. 4-6 Peak wavelengths of LEDs in the same bin to test the built-in errors.

Table 4-4 Built-in color errors by a width of peak wavelength in the same bin.

Peak wavelength (nm)	Color coordinate (u'v')
(1) Mixed LEDs of single bin	0.1886,0.4615
(2) 457.7	0.1901,0.4604
Difference between (1) & (2)	0.0019
(3) 460.0	0.1887,0.4635
Difference between (2) & (3)	0.0020

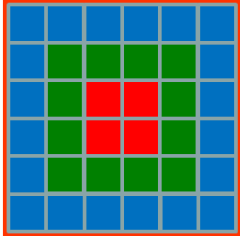
4.1.5 Boundary effect by light reflection

The last step is discussing the boundary effect. The color uniformity was influenced since the light reflected by the panel frame. A diffuse white frame is to cause the diffuse reflection, and an absorption black frame is to mimic the situation that there is no boundary, as shown in Fig. 4-7, Fig. 4-8 (a) and (b).

By measuring the backlight systems, the color difference between these two types is compared in Table 4-5, where ϵ is defined as the color error value. According to the results, the ϵ in the outer rings is larger than the inner locations, which are far away from the boundary. Also, the black boundary model is more similar to the proposed approach, as shown in Table 4-6.

Table 4-5 Color difference between the white boundary and black boundary modules.

	Avg.	Max.
$\epsilon_{1\text{st-circle}}$	0.0199	0.0201
$\epsilon_{2\text{nd-circle}}$	0.0222	0.0243
$\epsilon_{3\text{rd-circle}}$	0.0281	0.0334



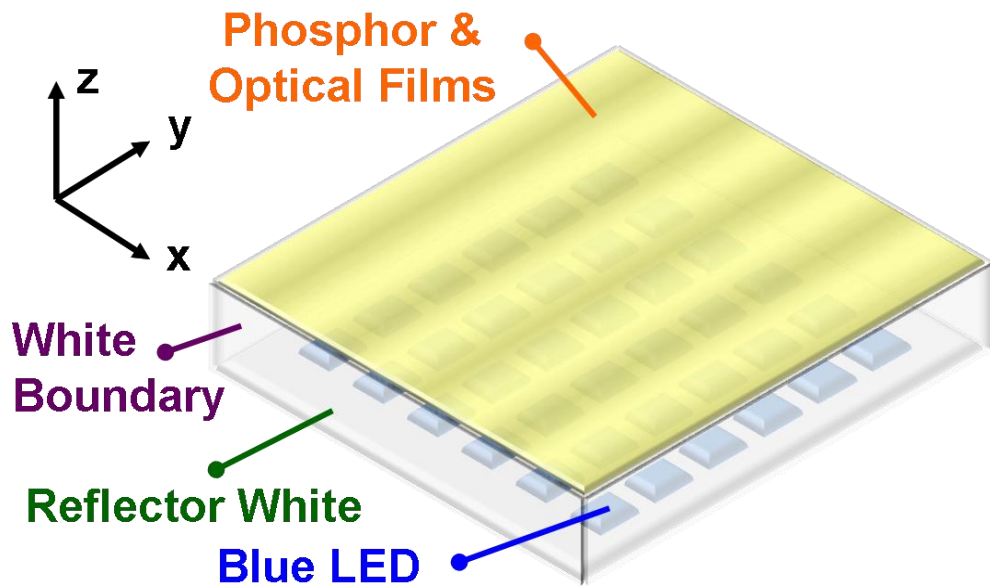


Fig. 4-7 Prototype with white boundary.

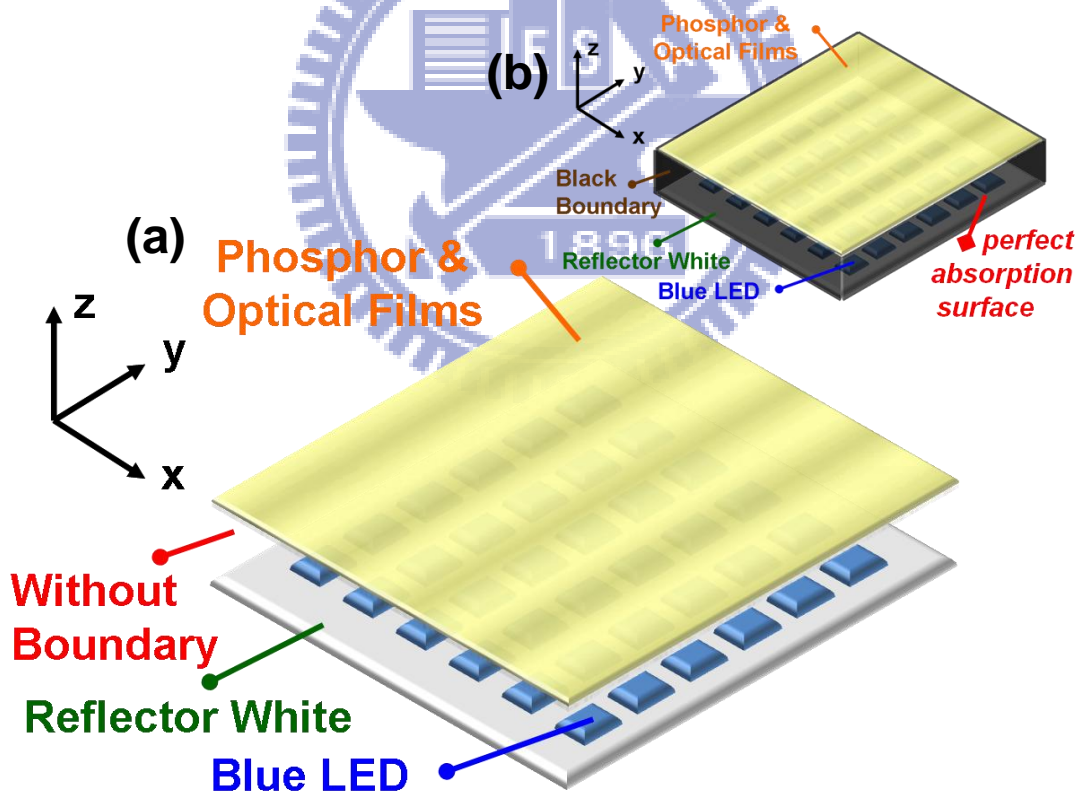


Fig. 4-8 Prototypes (a) without boundary; and (b) with black boundary.

Table 4-6 Color accuracy of simulation and black / white boundary prototypes.

Color errors with measurement	Black boundary	White boundary
$\Delta u'v'$ average	0.0041	0.0287
$\Delta u'v'$ maximum	0.0099	0.0338
$\Delta u'v'$ minimum	0.0003	0.0260

4.1.6 Total difference between calculation and experiment

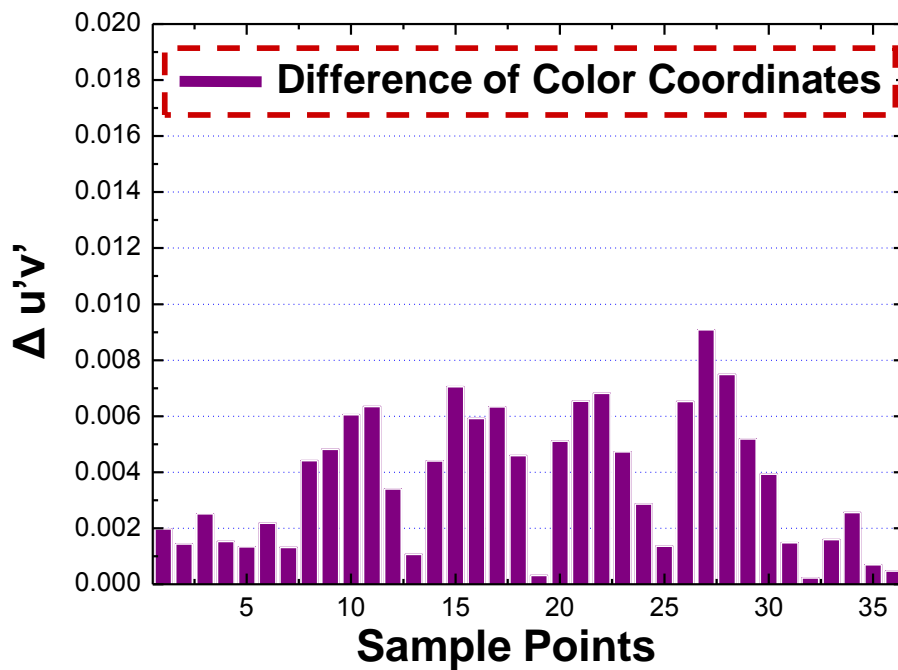


Fig. 4-9 Total differences between simulation and measurement in LUV color space.

All for all, combing all the steps of verification, we can find that the color deviation value by measuring 10-inch prototype is 0.0118, which is similar to the result of simulation one, 0.0196.

Moreover, by comparing the color difference between calculation and experiment, the average error value is ± 0.0019 and the maximum error value is 0.0087, which is small enough to verify the accuracy of calculation model, as shown in Fig. 4-9.

4.2 Summary

After comparing simulated results and measured data of prototype, the maximum error value is 0.0087 in CIE 1976 LUV color space, which is acceptable but could be reduced. Therefore, the simulated module was classified to many parts to analyze errors step by step. According to the results in this chapter, the color errors are small enough in the steps of correctness of LSF superposition method, and tolerance of self-fabricated module. Moreover, the tolerances of bin width are built-in errors, which could not improve anymore. However, the errors caused from affected color composition range of LED cannot be ignored. All these errors are attributed to reflected light by diffuser plate and reflector white. It means that the distance of emitted light guiding in module cavity is longer than predicted value, as shown in Fig. 4-10. Accordingly, to enhance the accuracy of proposed method, the affected intensity ratio of far LEDs must be considered when calculating the color coordinate in backlight system. Finally, designing the boundary effect, the black frame is to mimic the situation that there is no boundary. In this structure, the results are more similar to the proposed approach since there are without the unpredictable reflected light.

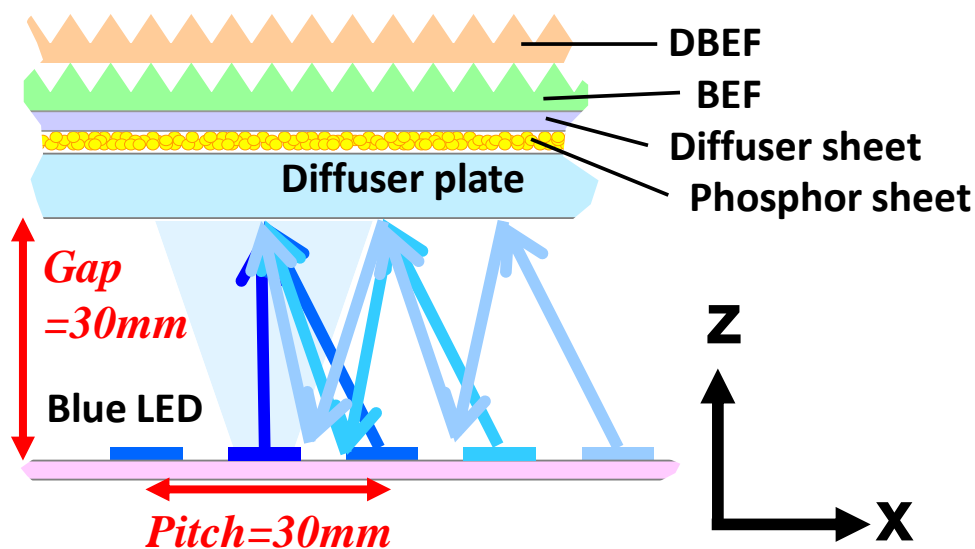


Fig. 4-10 Effected LEDs light by multi-reflection between reflector and diffuser plate.

Chapter 5

Results

After the verification of the calculation model, the color uniformity of backlight system could be computed handily in any conditions. The compositions of this chapter could be briefly classified to three parts. The first part is to calculate the color uniformity of backlight system with LED random arrangement. Furthermore, with the same conditions, the optimized best arrangement of different binned-LEDs designed to get the highest color uniformity is analyzed in the second part. Finally, some ideas of reducing gap were proposed.

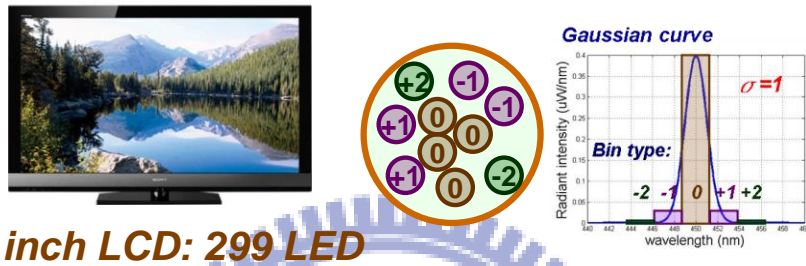
5.1 Random arrangement

The color uniformity of backlight system with random arrangement would be calculated by controlling the width of Gaussian function, σ , which fixing the amount ratio of different binned LEDs, in the steady module structure. This condition was simulated as the LEDs which manufactured by factories were directly used in the backlight system without classified the bin.

There are two LEDs sampling methods, as shown in Fig. 5-1 and Fig. 5-2. One is selecting the exactly number of each binned LEDs, which is controlled by the waist of the Gaussian function σ . The other way is that so many LEDs are collocated by the fixed ratio of bins, and randomly chooses the required LED amount. This method simulates the procedure of selecting backlight LEDs in the factory. So the LED amount of each bin is not equal in these two methods.

The results are analyzed by two different approaches. One is the statistics of color deviation which including the maximum, minimum and average data by computing 100 times. The other one is to calculate the worst case in the fixed conditions, which is occurred rarely in practical cases.

④ Selecting LEDs exactly number Method



32 inch LCD: 299 LED

Fig. 5-1 Amount binned- LEDs of selecting LEDs exactly number method.

④ Picking up LEDs randomly Method

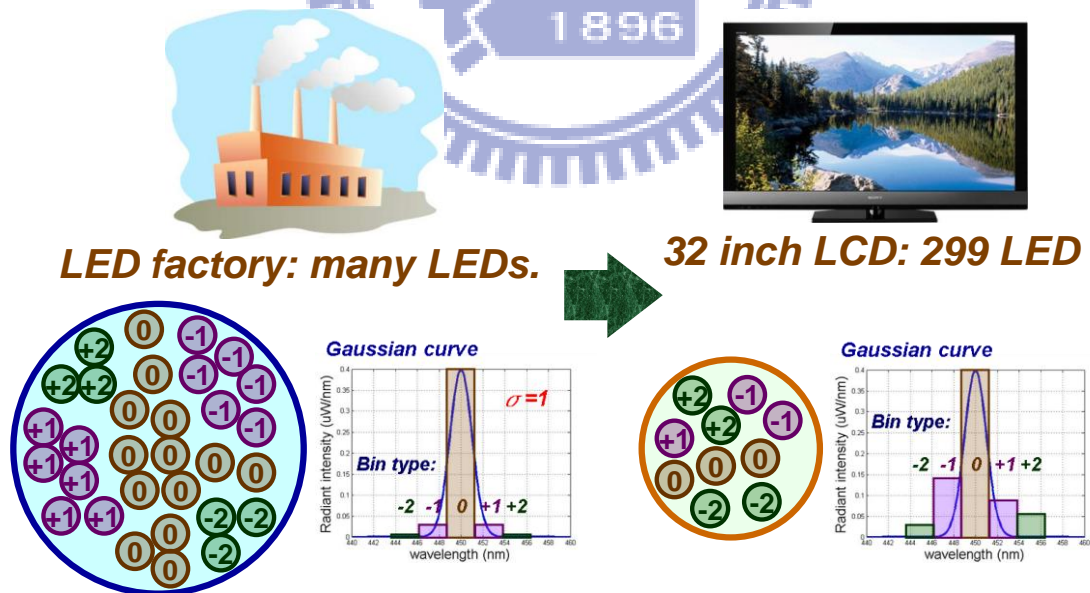


Fig. 5-2 Amount binned- LEDs of picking up LEDs randomly method.

In the simulation process, the conditions of module were the same as in the verification part, as shown in Table. 5-3. But the panel size of backlight was selected in 32 inch, which included 23x12 blue LED chips array. The arrangement of different bin LEDs in the LCD was random; in other words, the results were not always the same in different simulated times. The waist of the Gaussian function, σ , could be chosen as any values in different cases in simulation.

Both the peak wavelength and the intensity of LED influence the color uniformity of backlight, and the LED numbers distributed along the two binning factor have the characteristics of normal distribution. So we define the σ_1 and σ_2 values as the Gaussian waist of the different bins classified by peak wavelength and intensity.

According to the statistic value of LED factories, the σ_1 varied from one to four, as shown in Table 5-1, and the σ_2 was fixed as four.

Table 5-1 Conditions of simulation in LSF approximation method.

Wavelength (nm)				
-2nd	-1st	0th	+1st	+2nd
450~452.5	452.5~455	455~457.5	457.5~460	460~462.5

Intensity	Other parameters	
Bin width	Simulated times	Cost time
5%	100	90 minutes

5.1.1 Results of LEDs random arrangement:

(A) Method: select binned LEDs amount exactly; Arrangement: random

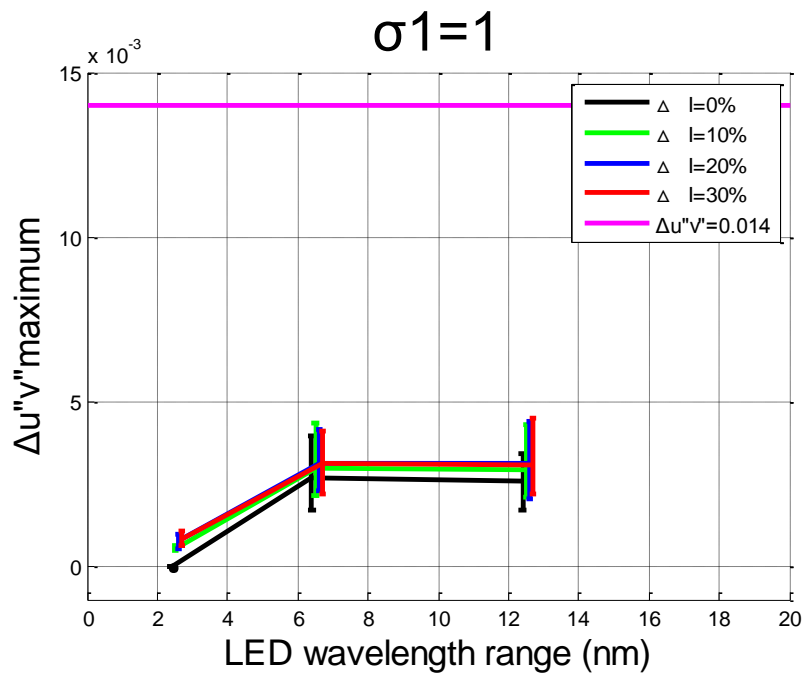


Fig. 5-3 Color deviation with $\sigma_1=1$ in selecting LEDs exactly method.

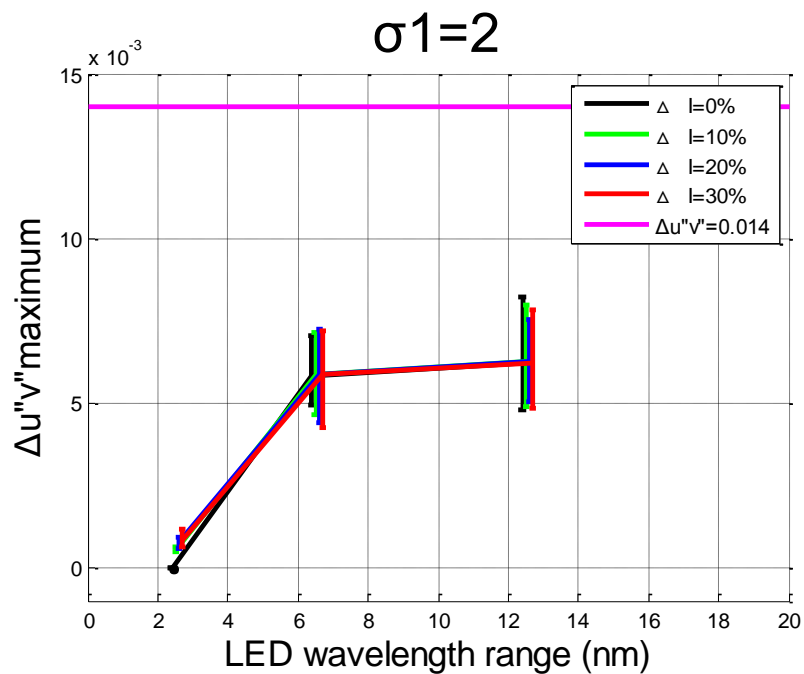


Fig. 5-4 Color deviation with $\sigma_1=2$ in selecting LEDs exactly method.

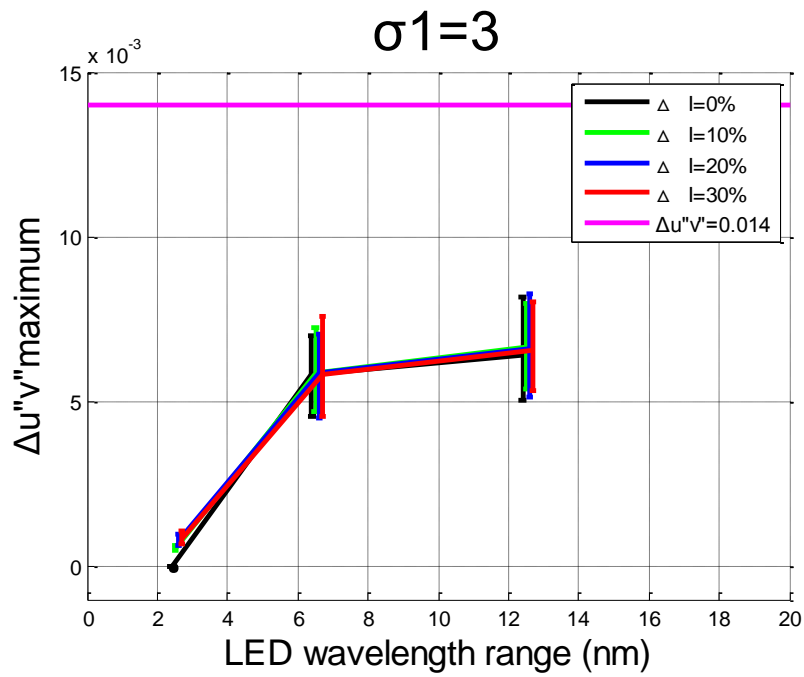


Fig. 5-5 Color deviation with $\sigma_1=3$ in selecting LEDs exactly method.

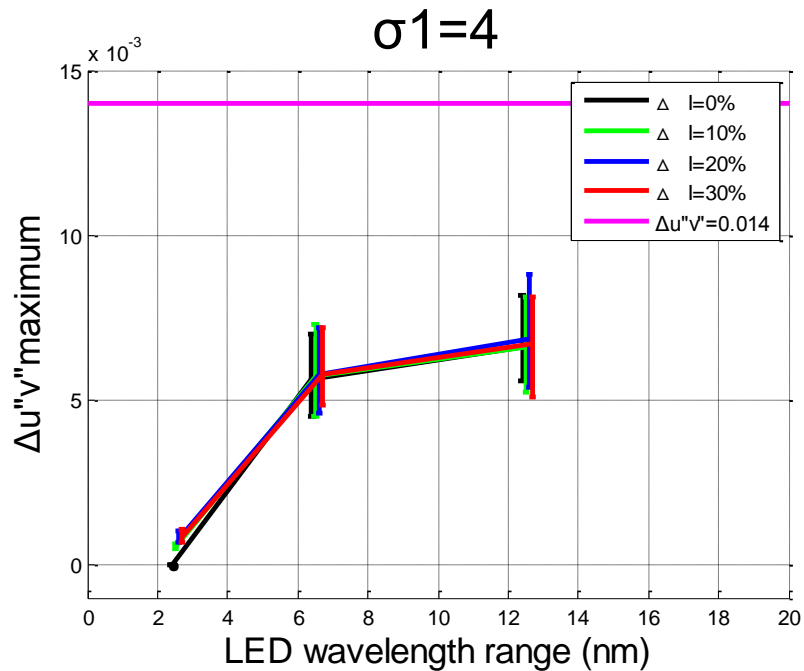


Fig. 5-6 Color deviation with $\sigma_1=4$ in selecting LEDs exactly method.

(B)Method: select binned LEDs amount randomly; Arrangement: random

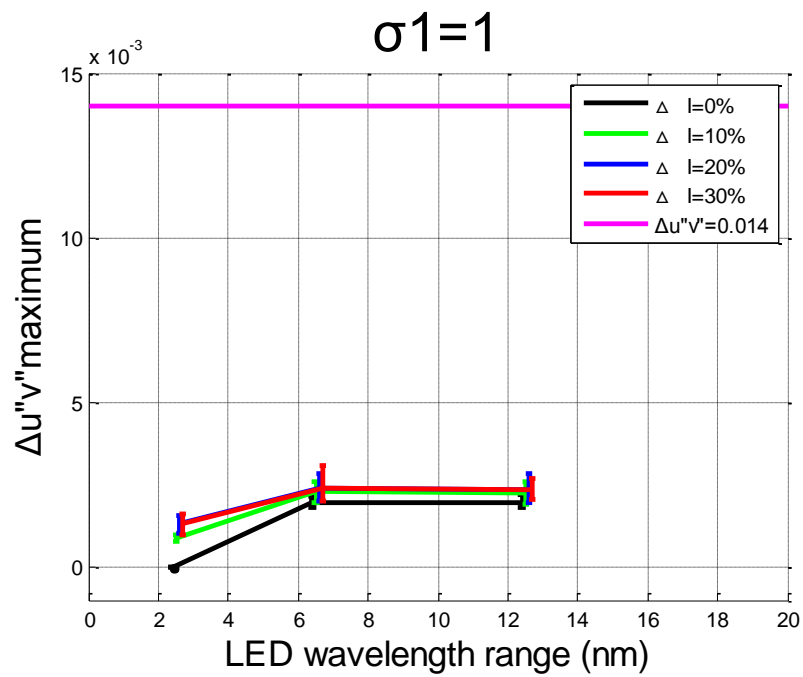


Fig. 5-7 Color deviation with $\sigma_1=1$ in picking up LEDs randomly method.

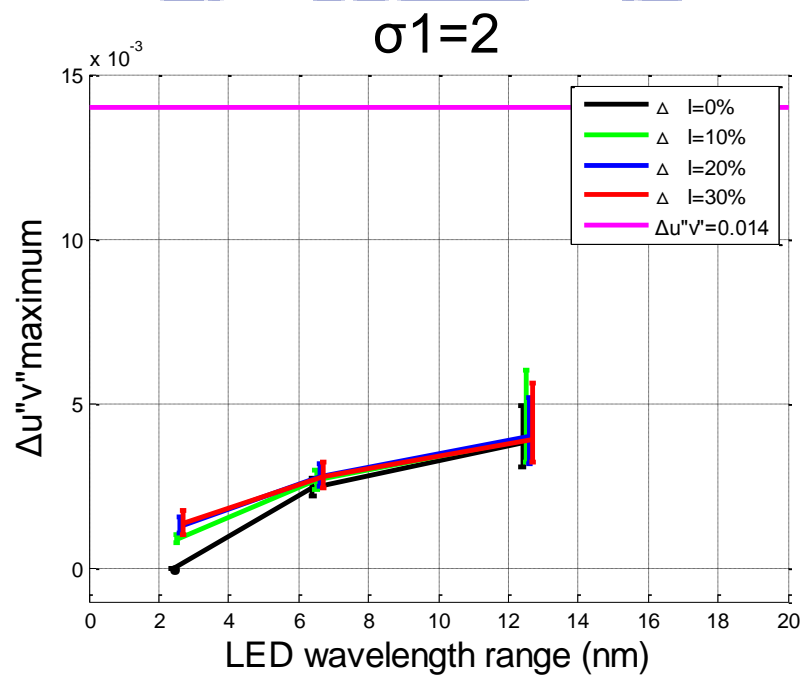


Fig. 5-8 Color deviation with $\sigma_1=2$ in picking up LEDs randomly method.

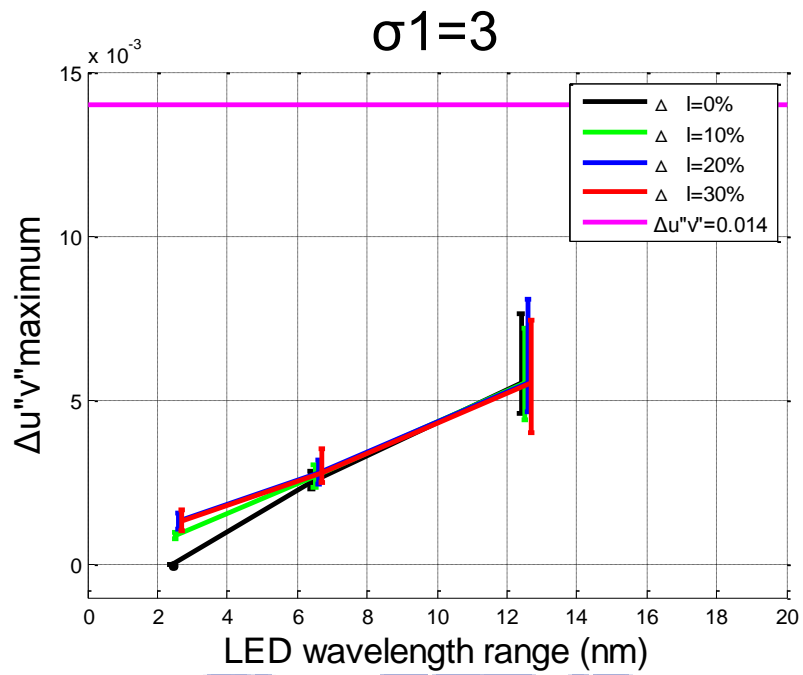


Fig. 5-9 Color deviation with $\sigma_1=3$ in picking up LEDs randomly method.

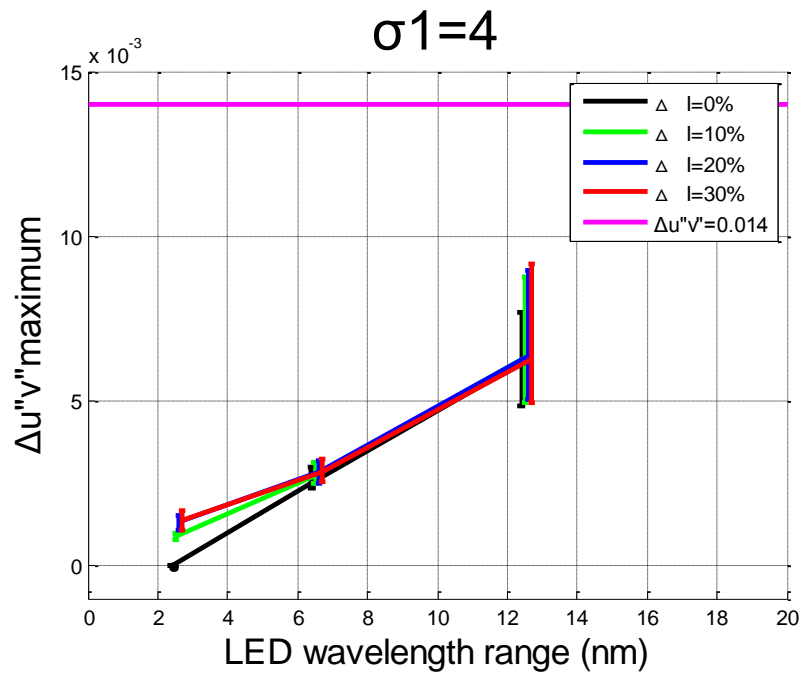


Fig. 5-10 Color deviation with $\sigma_1=4$ in picking up LEDs randomly method.

(C) Method: select binned LEDs amount exactly; Arrangement: worst case

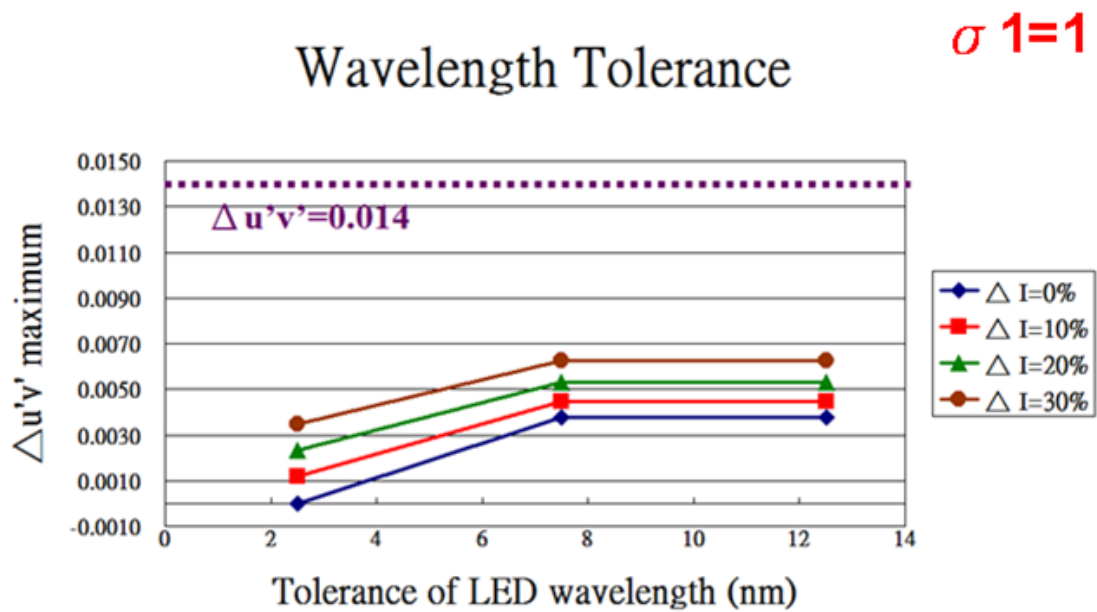


Fig. 5-11 Color deviation with $\sigma 1=1$ in the worst case.

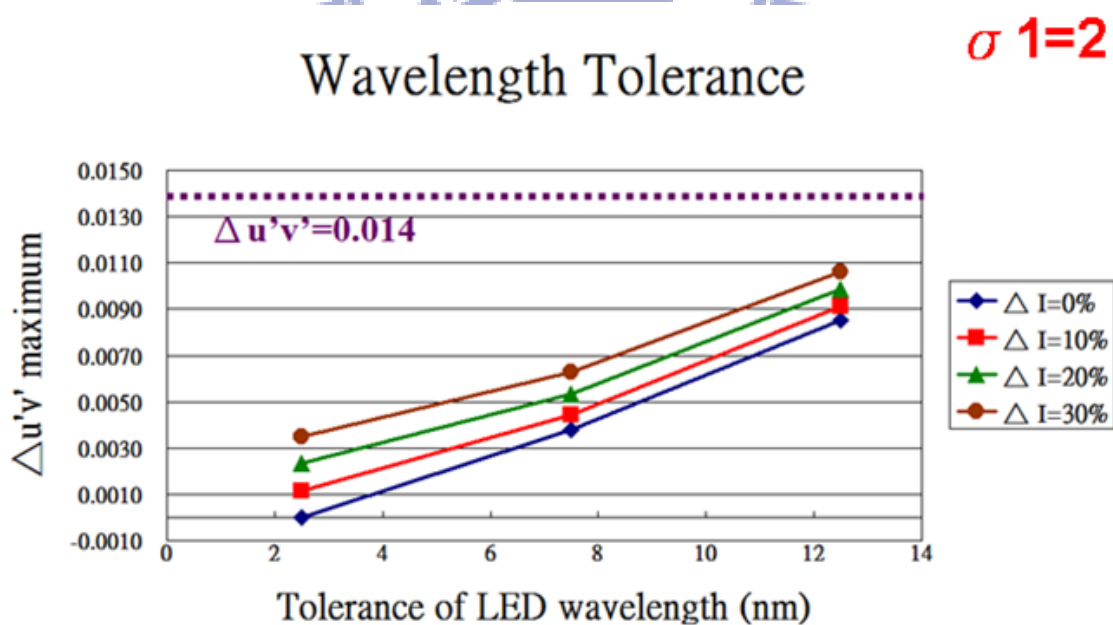


Fig. 5-12 Color deviation with $\sigma 1=2$ in the worst case.

Wavelength Tolerance

$\sigma 1=3$

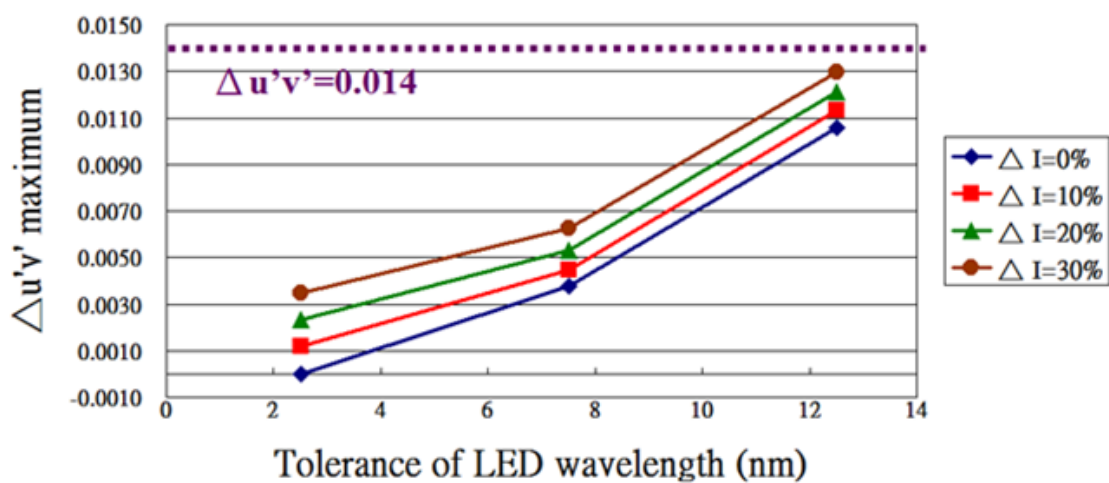


Fig. 5-13 Color deviation with $\sigma 1=3$ in the worst case.

Wavelength Tolerance

$\sigma 1=4$

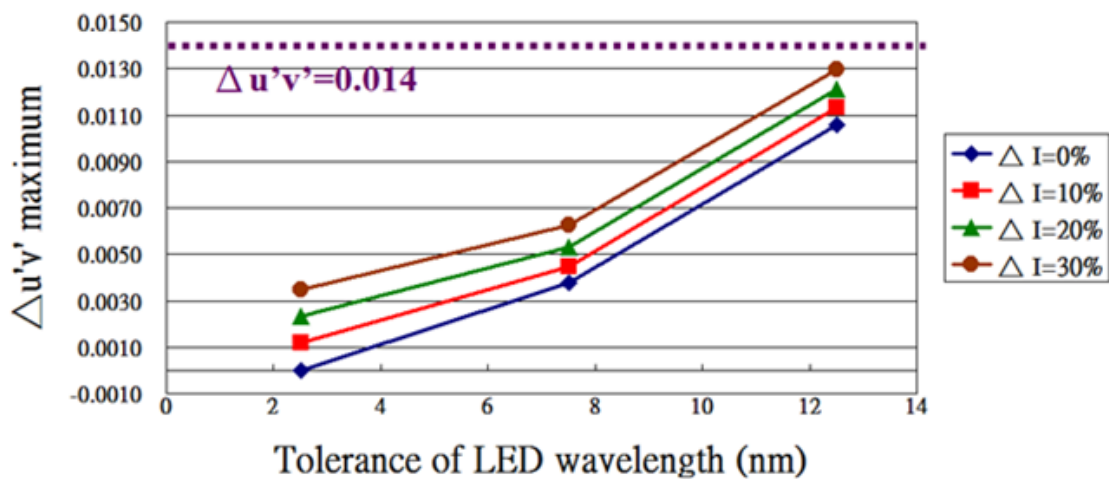


Fig. 5-14 Color deviation with $\sigma 1=4$ in the worst case.

5.1.2 Discussion:

With the given structure of direct-emitting backlight, the color uniformly was simple simulated by this method. Also, the best backlight binned LEDs arrangements of simulating 100 times were obtained. Moreover, the color coordinates of the positions above every LED in the whole panel were also calculated. Therefore, whether the color deviation was acceptable in these fixed conditions could be simply found.

Comparing and analyzing the results as shown above, firstly, the $\Delta u'v'=0.014$ curve is defined as the acceptable color deviation of backlight system in this thesis. When the waist of Gaussian curve, σ_1 , is wider, the LED numbers of the edge bins are larger inducing worse color uniformity. Generally, the worst case (see Fig. 5-11 – Fig. 5-14) in the fixed conditions is occurred rarely since few edge binned-LEDs need to be arranged nearby each other. Because the binned ratio of LEDs is fixed and stable when the Gaussian waist is wide enough, the curves of $\sigma_1=3$ and $\sigma_1=4$ are almost the same in the worst case. In the selecting the exactly number of each binned LEDs method (see Fig. 5-3 – Fig. 5-6), the color deviations are larger than in picking up LEDs randomly method (see Fig. 5-7 – Fig. 5-10) when the total bin width is 7.5nm or 12.5nm. This phenomenon is occurred from the amount of edge binned-LEDs, which is fixed in the selecting exactly method and may be zero in selecting randomly method, probably.

However, since the arrangement was random, the color uniformity would be changed case by case. For the minimizing color deviation purpose, we proposed the method of optimized LED arrangement further.

5.2 Optimized arrangement

The purpose is to optimize the best arrangement of different binned-LEDs, where had the highest color uniformity. Attributing to the too much ways of the arrangements, we use the 3×3 LEDs superposition method in this part to reduce the calculated time, which was different to the random simulation case.

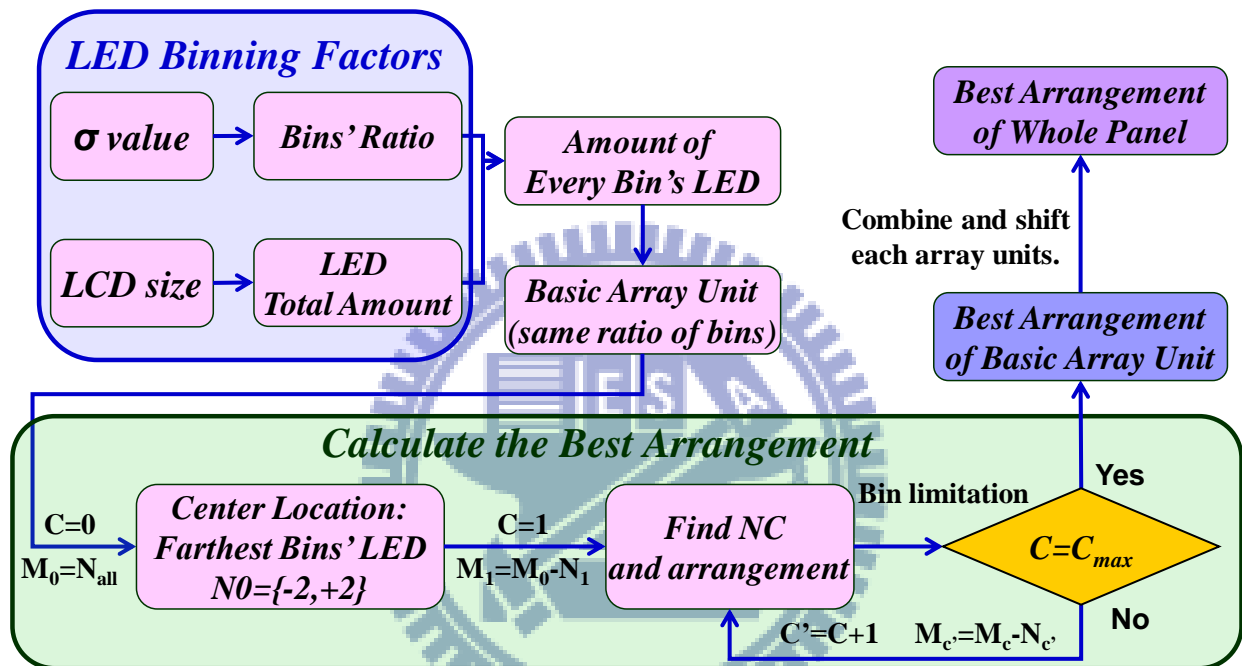


Fig. 5-15 Flowchart of the optimized arrangement method.

Fig. 5-15 shows the flowchart of optimized arrangement. The first step is to fix the LED binning factors, which represent the LED amounts of different bins. When the width of Gaussian function σ is defined, the count of each binned LEDs could be obtained. Then the sum of total LEDs is easily calculated by clarifying the size (inch), the gap (h) and the pitch (p) of the panel. In the simulation, the σ equaled 2, the size of the panel was 32 inches, and both the gap and pitch were 30 millimeter. The wavelength binning distribution was the same as that in the previous case.

Basing on these definitions, the number of the LED distribution should be defined

as

$$M(n) = R'(n) \times C, \quad (5.1)$$

where the C is the integer corrective factor. Therefore, the basic LED amount is dominated by the summation of M , which indicates that the LEDs quantity of each bin is an integer and as small as possible, when the ratio of total would be kept. Basing on the basic LED amount,

$$\sum_n M(n), \quad (5.2)$$

which can be summed by each binned LEDs, we can find the rectangular unit array to arrange. The LED amount should be satisfied the geometrical condition of the considered unit array.

In the Fig. 5-16, the number of each $3 \times 3 \text{ cm}^2$ grille indicates the bin type of LED, which located in the center of grid. Also, the amount of $\pm 2^{\text{nd}}$ binned-LED is just one in this figure.

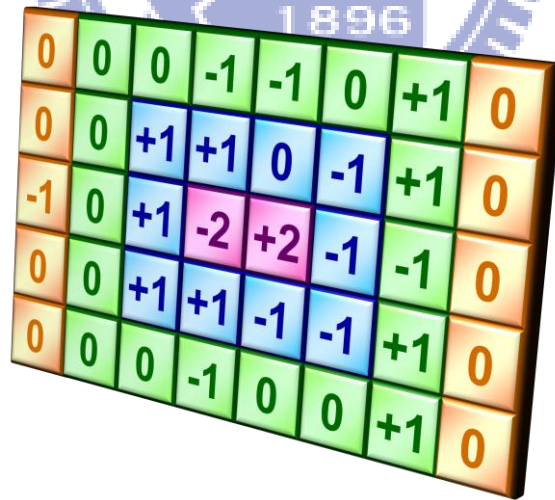


Fig. 5-16 Optimized arrangement of each bin in basic unit array.

First, the LEDs of the edge bins, which have the largest interval in the color coordinates, are placed on the center of a basic unit array and nearby each other for the

purpose of color balance. Then the LEDs of the more inner bin should be arranged efficiently on the wider concentric circle until the center binned LEDs were arranged on the most outer ring. In each considered circle, all cases of LED arrangements were discussed. Through this rule, the best arrangement of one basic array unit could be derived. As shown in Fig. 5-17, the arrangement of whole panel can be formed by the combination of the multiple unit arrays. The last step is to shift the relative position of each basic unit array to eliminate the non-uniform effect on the boundary.

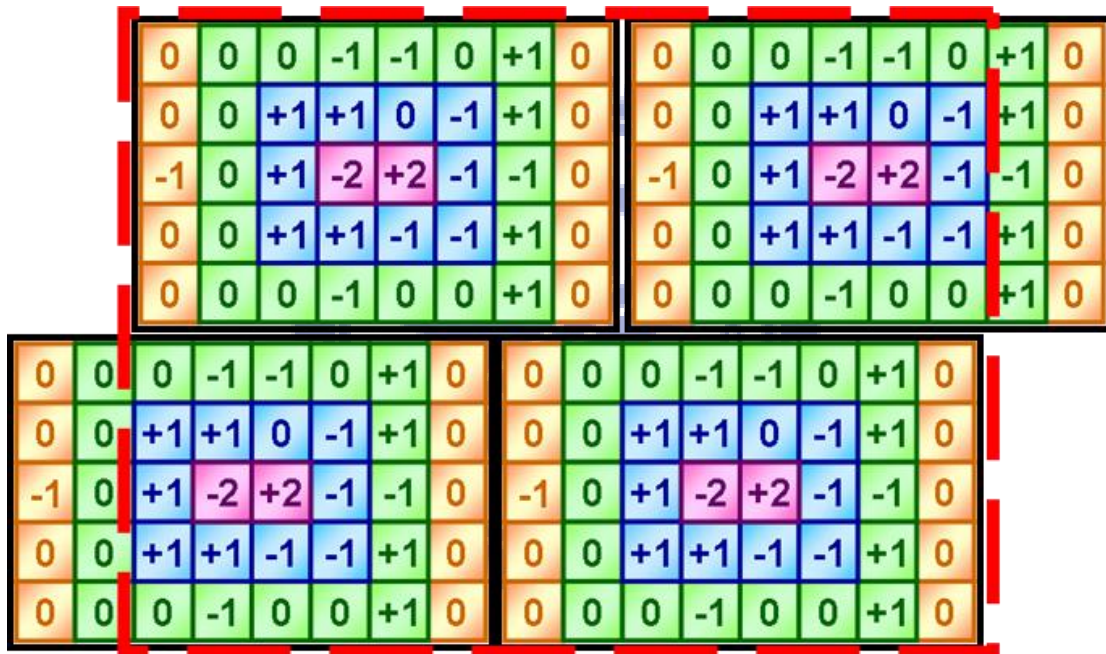


Fig. 5-17 Arrangement of whole panel with considering boundary effects.

Moreover, the prototype of optimized LED arrangement was built, and demonstrated the high color uniformity, as shown in Fig. 5-18. Compared with average color deviation, 0.0054, in the random arrangement with three of σ_λ , the optimized one was 0.0030, which definitely improved the color characterization of direct-emitting backlight, as shown in Fig. 5-19 (a) and (b).

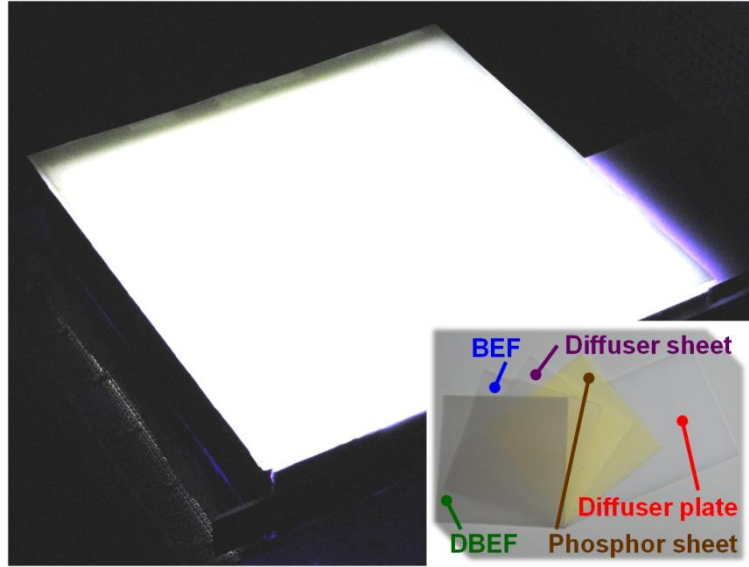


Fig. 5-18 Optical films and illuminating prototype of optimized LEDs arrangement.

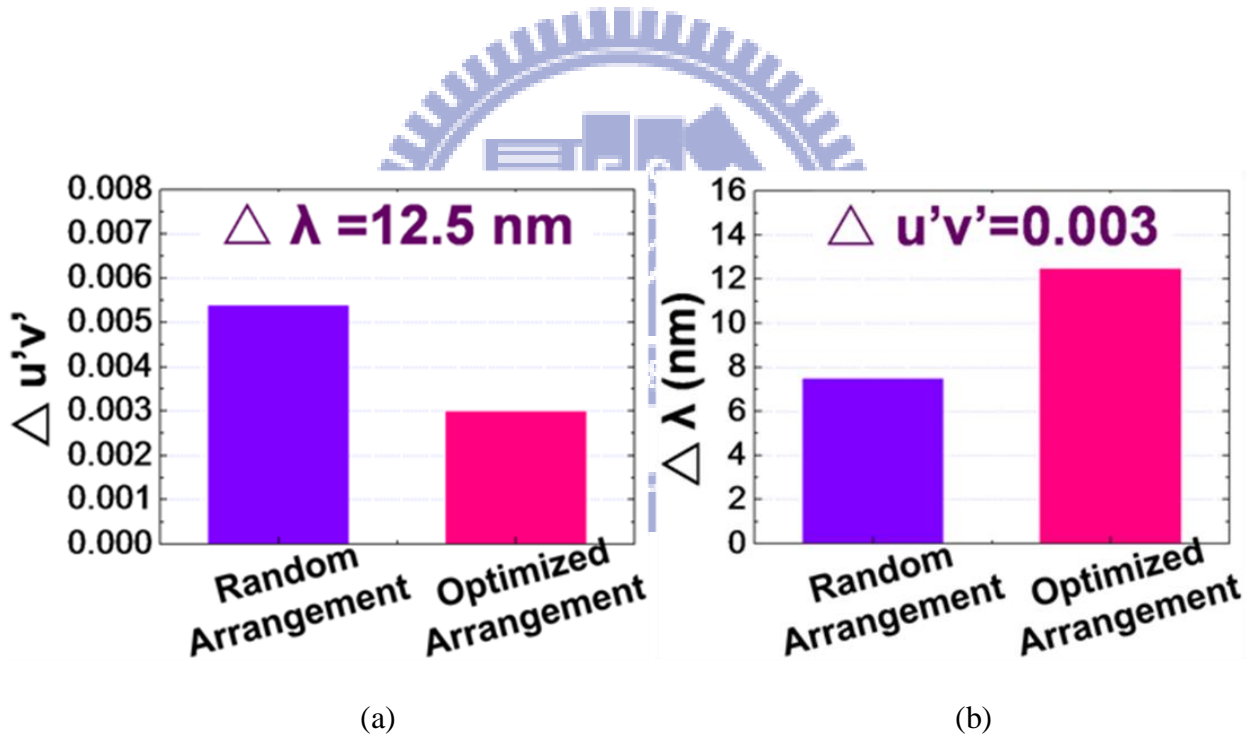


Fig. 5-19 Enhanced color uniformity of optimized arrangement than random arrangement with fixing (a) total wavelength range; (b) color deviation.

5.3 Method for reducing gap

In this project, the module gap of prototype is 30 millimeter. To reduce model gap is the main purpose of this section. By changing the LED angular distribution, we can produce the similar LSF under reduced module gap, which is illustrated in Fig. 5-20 (a) and (b).

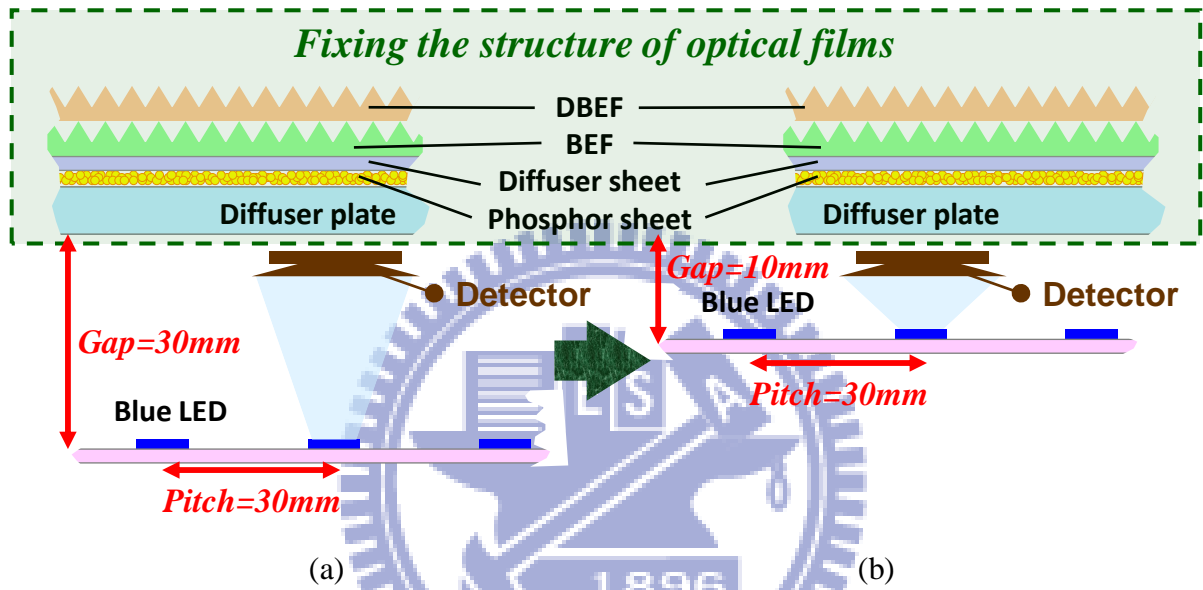


Fig. 5-20 Simulated structures with (a) gap=30mm; and (b) gap=10mm.

According to the photometry, the illuminance E_d projected from a LED source with distance z can be written as

$$E_d = \frac{d\Phi_d}{dA_d} = I_s \frac{dA_d \times \cos \theta}{dA_d \times r^2} = I_s \frac{\cos \theta}{(z / \cos \theta)^2} = I_s \frac{\cos^3 \theta}{z^2}, \quad (5.3)$$

where I_s is the luminous intensity of a LED, and θ is the angle between the considered area and the source normal. In general cases, I_s is Lambertian distribution, $I_0 \cos \theta$. The geometrical parameters are schematically illustrated in Fig. 5-21.

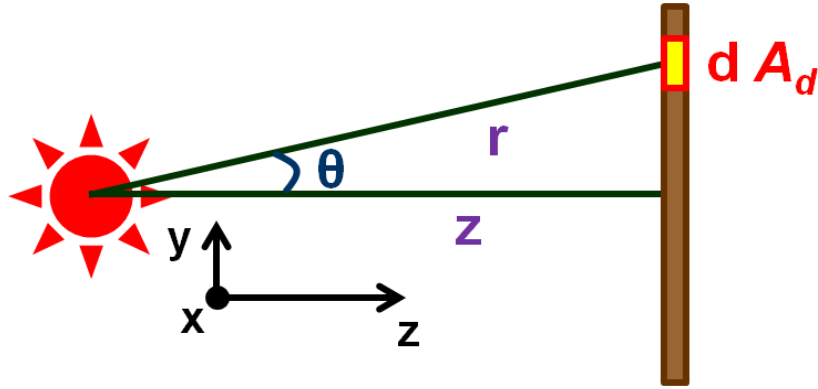


Fig. 5-21 Detected area of analyzed structure in Photometry.

Through the scatter and emission property, the illuminance E_d on the phosphor sheet is proportional to LSF. We assume the $LSF_{z=30}$ under $z = 30$ mm as a target distribution $LSF_{z=30}$. Thus, the expected intensity I' under a reduced gap z' can be inversely derived from the target distribution

$$\frac{I'(\theta') \times \cos^2 \theta'}{z'^2} = \frac{I_0 \times \cos^3 \theta}{z^2} \Big|_{z=30} = LSF_{z=30} \quad (5.4)$$

The relationship between θ and θ' is illustrated as

$$z \tan \theta = z' \tan \theta' \Rightarrow \theta' = \tan^{-1} \frac{z}{z'} \tan \theta \quad (5.5)$$

Therefore, $I'(\theta)$ under 10-mm gap is derived as the distribution shown in Fig. 5-22 (a) and (b).

Based on the calculated light emitting shape of LEDs, the commercial light tracing software, Light Tools, was used to reproduce the LSF. The two commercially available LED packages (in Fig. 5-23 (a) and (b)) were chosen as the light sources in these two conditions. The reproduced LSFs are compared in Fig. 5-24. The close agreement shows the LED with batwing intensity pattern can keep the LSF and replaces for the 10-mm gap application.

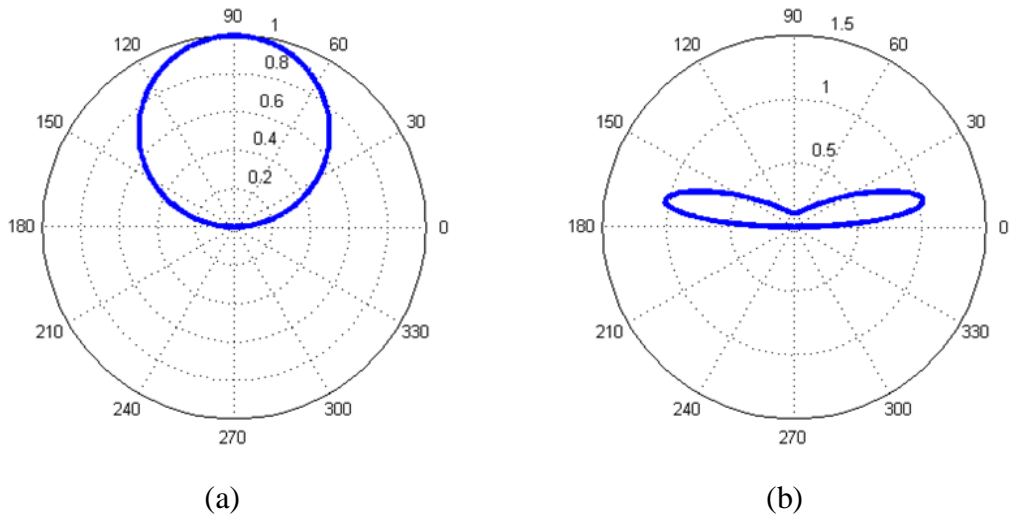


Fig. 5-22 Emitting light shapes of (a) normal LEDs (module gap=30mm); and (b) calculated LEDs (module gap=10mm).

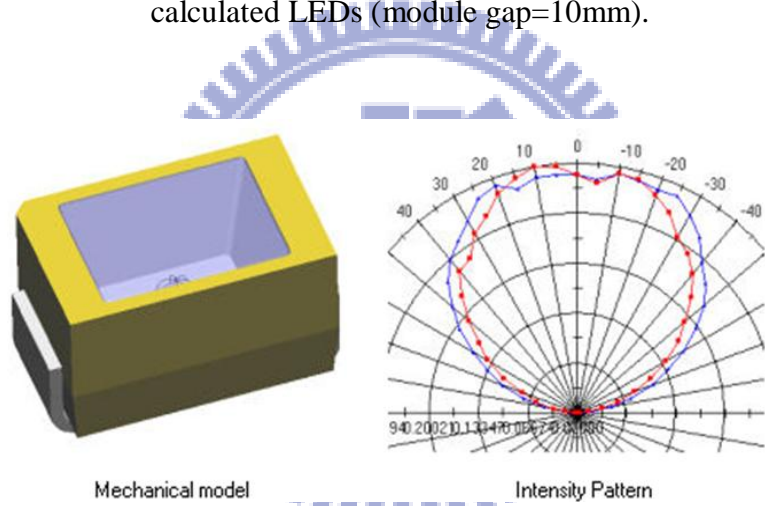


Fig. 5-23 Emitting light shape of real LEDs in the commercial when gap=30mm.

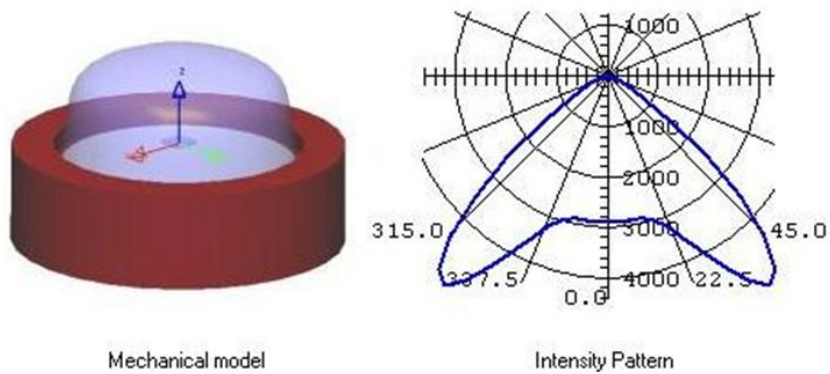


Fig. 5-24 Emitting light shape of real LED in the commercial when gap=10mm.

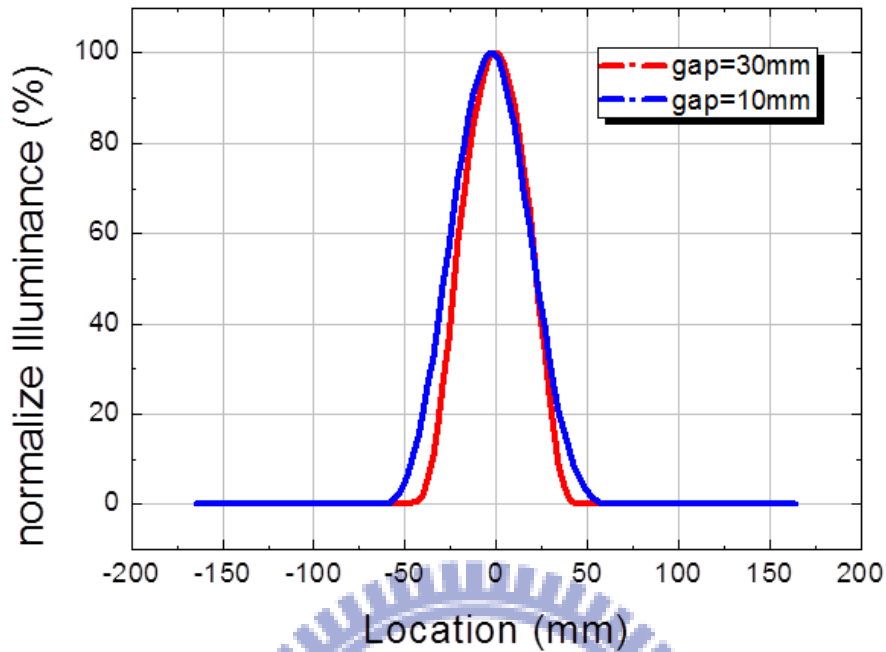


Fig. 5-25 Simulated illuminances in software with 30mm and 10mm module gaps.

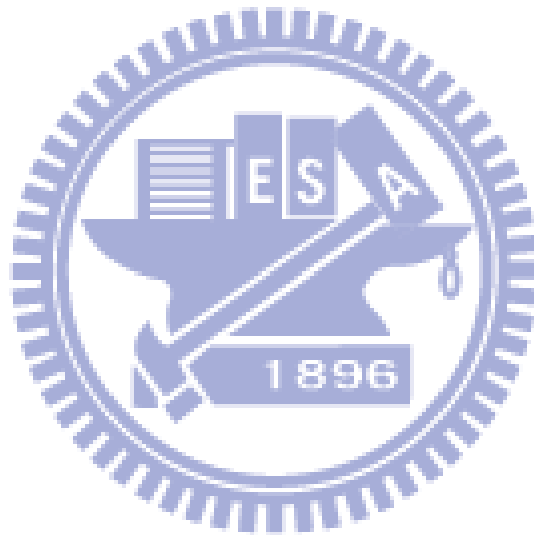
5.4 Summary

In this chapter, the simulated results could be classified to three parts. The first part is to calculate the color deviation of backlight system with binned-LEDs random arrangement. All methods of the worst case, selecting LEDs exactly number, and picking up LEDs randomly were completed and analyzed. From these results, the color uniformly was simple simulated with the given structure of direct-emitting backlight. Therefore, whether the color deviation was acceptable in these fixed conditions could be simply found.

The second part is discussing the optimized LED arrangement to minimize color deviation, furthermore. Based on keeping the ratio of total amount and dividing the greatest common divisor, the unit array would be obtained and the different binned-LEDs were arranged from center to the most outer circle efficiently by color

complementary. According to the results of simulation, the color deviation, $\Delta u'v'$, was reduced from 0.0054 to 0.0030 by using optimized LEDs arrangement with keeping total bin types. In the other words, basing on this method, the range of usable bin wavelength could be enhanced from 7.5nm to 12.5nm with fixing acceptable color deviation.

The final part is to discuss the method of reducing module gap. Basing on the Photometry, the emitting light shapes of LEDs would be designed to keep the same illuminance of backlight output with fixing optical films and optical properties.



Chapter 6

Conclusions and Future Work

6.1 Conclusions

Slim format LCDs has been widely used in the current display market. To display high quality images from LCDs, direct-emitting backlight systems are used to provide sufficient bright and uniform light source for the LC panel. Moreover, LED is expected to become the major backlight source now because of enhanced energy efficiency, a larger lifetime, the omission of mercury, and compliance with demand for green technologies. Since the manufacturing effect, LEDs are classified to different bin types by wavelength, brightness, and voltage. However, the wavelength requirement of LED is very strict in LCD backlight.

To solve this issue and extend the usable range of binned-LEDs, the LSF approximation method was built to analyze the optical properties and color deviation of direct-emitting backlight system. Also, the remote phosphor technology, which has the benefits of high optical efficiency and uniformity, was used. In this thesis, the LSF approximated method, which requiring the luminance and spectrum data of single LED, was proposed. By using the idea of light mixing and superposition, the color uniformity information of backlight could be simulated simply. Comparing the simulation with experiment, the average color difference between them is ± 0.0019 . Moreover, after verifying, the 5×5 approximation is more suitable to simulate the color deviation.

In the software, the remote phosphor sheet direct-emitting backlight system was set up, which composed of blue LED chips, reflector white, diffuser plate, phosphor

sheet, diffuser sheet, BEF and DBEF. In the simulation, the module gap (h) and the period of blue LED chips (p) were both 30 mm. The range of blue LED peak wavelengths in the center bin (0^{th}) was from 455.0 nm to 457.5 nm, and the others were every 2.5 nm nearby the center one.

For the random arrangement results, the LED binning distribution, which be sorted by wavelength and flux, is described by the Gaussian function. The results of random arrangement with selecting LEDs exactly and selecting LEDs randomly were accomplished, where the largest color deviations are similar to 0.009 in the conditions with σ_1 equaling 4 and 12.5nm LED wavelength range. Moreover, the maximum color deviation of LED worst arrangement that selecting LEDs amount exactly is about 0.013, which is smaller than the limited value, 0.014. Furthermore, the best backlight arrangements of binned LEDs are also obtained, where the simulation times is 100.

For the optimized arrangement results, the LEDs of the edge bins are placed on the center of a basic unit array and nearby each other for the purpose of color balance. The more inner bin should be arranged efficiently on the wider concentric circle until the center binned LEDs were arranged on the most outer ring. Then the relative position of each basic unit array is shifted to eliminate the non-uniform effect on the boundary. According to the simulation results, the color deviation by using the optimized arrangement method could be reduced about 0.002 than the random arrangement with the same conditions.

For the reducing gap method, by simulating the new LED angular distribution with fixing all optical films in the light tracing commercial software, Light Tools, the optical characteristics of module cell gap=10mm are similar to that of gap=30mm since the alike illuminances of backlight.

6.2 Future works

The LSF approximation method was developed successfully to analyze the optical properties and color deviation of direct-emitting backlight system. However, basing on the convenience to use widely, there are some issues to be improved. The first one is to build a relative function between LSF and spectrum. Since the spectral radiance has varied composition on different locations and viewing angles, the spectrometer needs to move in the necessary places when measuring the spectrums. By building the relative function of LSF and spectrum, the spectrums could be inserted in everywhere and the measured time and data would be reduced.

The second one is reducing the system errors by superposition more effected spectrums of LEDs when calculating the color coordinates of backlight. According to the relative function of LSF and spectrum, the spectrums of far LEDs could be inserted by calculation and considered in the convolution process to solve the problem that the distance of guiding light in module cavity is longer than predicted.

Recently, the technologies of side-emitting backlight system are grown suddenly and are widely used in LCDs. In response to the trend of the times, an efficient calculation system to analyze the side-emitting backlight optical properties and color deviation is needed to build by the similar processes of LSF approximation method.

References

- [1] S Nishigaki et al, "Plasma display panel", US Patent 5,209,688 (1993)
- [2] Dawson, R.M.A. et al, "The impact of the transient response of organic light emitting diodes on the design of active matrix OLED displays", IEDM '98 Technical Digest, p.875 (1998)
- [3] W. B. Choi et al, "Fully sealed, high-brightness carbon-nanotube field-emission display", Applied Physics Letters, Vol. 75 (1999)
- [4] J. I. Pannkove, "Display Devices (Topics in Applied Physics)", Chap.4, Springer-Verlag (1980)
- [5] E. Lueder, *Liquid Crystal Displays*, John Wiley & Sons, p.294 (2000)
- [6] H.-T. Huang, C.-H. Hung, Y.-P. Huang, C.-H. Tien, C.C. Tsai, H.-P. D. Shieh, J. Lin, J. Chen, P. Chen, and W.-C. Chang, "UV Excited Flat Lighting (UFL) System for LCD-TV Backlight Application," SID'08 DIGEST, p.862-p.865 (2008)
- [7] B.-W. Xiao, C.-H. Hung, H.-T. Huang, J. Chen, Y.-P. Huang, C.-H. Tien, and C.C. Tsai, "LEDs-based Flat Lighting Device for LCD Backlight Applications," OPT'08, Sat-S23-01 (2008)
- [8] B.-W. Xiao, C.-H. Hung, H.-T. Huang, Y.-P. Huang, C.-H. Tien, C.C. Tsai, H.-P. D. Shieh, J. Chen, J. Lin, and W.-C. Chang, "Optical Simulation and Analysis of Visible-light Excited Phosphor Sheet (VEPS) System," IDMC'09, Wed-P5-01 (2009)
- [9] B.-W. Xiao, C.-H. Hung, H.-T. Huang, Y.-P. Huang, C.-H. Tien, C.C. Tsai, H.-P. D.

- Shieh, J. Chen, J. Lin, and W.-C. Chang, "Optical Properties of Visible-light Excited Phosphor Sheet (VEPS) System," SID'09 DIGEST, p.1034-p.1037 (2009)
- [10] K. Kälantär, "Highly Light Collimating Unit for Realization of Mosaic Structure Large Size RGB Backlight," IDW'05, p.1273-1276 (2005)
- [11] E. Lueder, *Liquid Crystal Displays*, John Wiley & Sons, p.121 (2000)
- [12] J. Graf, G. Olczak, M. Yamada, D. Coyle and S. Yenug, "Backlight Film & Sheet Technology for LCDs," Seminar Lecture Note, SID'08, p.M-12/6 (2008)
- [13] N. Narendran, Y. Gu, J.P. Freyssinier-Nova, and Y. Zhu, "Extracting Phosphor-Scattered Photons to Improve White LED Efficiency," *Phys. Stat. Sol. (A)*, vol. 202, p. r60-r62 (2005)
- [14] D. Hreniak and W. Sterk, "Synthesis and Optical Properties of Nd³⁺ doped Y₃Al₅O₁₂ Nanoceramics," *Journal of Alloys and Compounds*, vol. 341, p.183-186 (2002)
- [15] H. Luo, J. K. Kim, E. F. Schubert, J. Cho, C. Sone, and Y. Park, "Analysis of High-Power Packages for Phosphor-Based White-Light-Emitting Diodes," *Appl. Phys. Lett.*, vol. 86, 243505 (2005)
- [16] S. C. Allen, and A. J. Steckl, "EliXIR-Solid-State Luminaire with Enhanced Light Extraction by Internal Reflection," *Journal of Display Tech.*, vol. 3(2), pp. 155-159 (2007)
- [17] S. C. Allen, and A. J. Steckl, "A Nearly Ideal Phosphor-converted White Light-emitting Diode," *Appl. Phys. Lett.* vol. 92, 143309 (2008)
- [18] LED binning map, <http://www.flickr.com/photos/protium/4133646743/>, (2009)
- [19] B. E. A. Saleh, and M. C. Teich, *Fundamentals of Photonics*, John Wiley & Sons, Inc, p.4 (1991)
- [20] E. Hecht, *Optics, 4th Edition*, Addison Wesley, p.100 (2002)
- [21] E. Hecht, *Optics, 4th Edition*, Addison Wesley, p.98 (2002)

- [22] S.O. Kasap, *Optoelectronics and Photonics: Principles and Practices*, Pearson Prentice Hall, p.18 (2001)
- [23] S.O. Kasap, *Optoelectronics and Photonics: Principles and Practices*, Pearson Prentice Hall, p.18 (2001)
- [24] W. J. Smith, *Modern Optical Engineering: The Design of Optical Systems, 3rd Edition*, Mc-Graw-Hill, p.219 (2000)
- [25] N. Ohta and A. R. Robertson, *Colorimetry: Fundamentals and Applications*, John Wiley & Sons, p.22 (2005)
- [26] 1988 CIE Photopic Luminous Efficiency Function,
<http://note.j-i-n.name/2005/06/photopic-luminous-efficiency-function>, (2005)
- [27] T. Smith and J. Guild, "The C.I.E. Colorimetric Standards and Their Use," *Transactions of the Optical Society* 33 (3), p. 73-134 (1931)
- [28] R. W. Hunt, *Measuring Colour, 3rd Edition*, Fountain Press, England, p. 39-57 (1998)
- [29] A. C. Harris and I. L. Weatherall, "Objective Evaluation of Colour Variation in the Sand-burrowing Beetle *Chaerodes Trachyscelides* White by Instrumental Determination of CIELAB Values," *Journal of the Royal Society of New Zealand*, 20(3) (1990)
- [30] N. Ohta and A. R. Robertson, *Colorimetry: Fundamentals and Applications*, John Wiley & Sons, p.76 (2005)
- [31] N. Ohta and A. R. Robertson, *Colorimetry: Fundamentals and Applications*, John Wiley & Sons, p.115 (2005)
- [32] N. Ohta and A. R. Robertson, *Colorimetry: Fundamentals and Applications*, John Wiley & Sons, p.119 (2005)
- [33] D. H. Alman, R. S. Berns, G. D. Snyder, and W. A. Larson, "Performance Testing of

- Color Difference Metrics Using a Color-Tolerance Dataset,” *Color Research and Application*, vol. 21, pp.174-188 (1989)
- [34] M. D. Fairchild, *Color Appearance Models*, Reading, Massachusetts, Addison-Wesley (1998)
- [35] J. Schanda, *Colorimetry: Understanding the CIE System*, Wiley Interscience, p. 61-64 (2007)
- [36] TCO'06 Media Displays, <http://www.tcodevelopment.com/>, (2006)
- [37] J. Santamaria, P. Artal, and J. Bescos, “Determination of the point-spread function of human eyes using a hybrid optical-digital method,” *Journal of the Optical Society*, vol. 4 (6), (1987)
- [38] ProMetric PM-1600 Imaging Colorimeter, <http://www.pro-lite.co.uk/File/PM-1600.php>, (2012)
- [39] B. E. A. Saleh, and M. C. Teich, *Fundamentals of Photonics, 2nd Edition*, John Wiley & Sons, Inc, p. 695 (2007)
- [40] Topcon SR-UL1R, <http://www.totalsmart.com.tw/>, (2011)
- [41] Y. Ito, T. Tsukahara, S. Masuda, T. Toshida, N. Nada, T. Igarashi, T. Kusunoki, and J. Ohsako, “Optical Design of Phosphor Sheet Structure in LED Backlight System,” *SID'08 DIEST*, p.866-869 (2008)
- [42] H. Guo, “A Simple Algorithm for Fitting a Gaussian Function,” *IEEE* (134), (2011)

Publication List

International Conference Papers

1. **Ping-Yen Chou**, Yi-Pai Huang, Chien-Hsiang Hung, and Yasushi Ito, “Optimization of LED Arrangement for Extending LED Binning Range in Backlight System,” The Society Information Display 2012 (SID 2012, Oral)

Domestic Conference Paper

1. **Ping-Yen Chou**, Yi-Pai Huang, Chien-Hsiang Hung, and Yasushi Ito, “Optimization of LED Arrangement for Extending LED Binning Range in Backlight System,” Taiwan Display Conference 2012 (TDC 2012, Poster)

